Volume 15
Number 29
7 August 2024
Pages 2925-3020

Polymer Chemistry

rsc.li/polymers

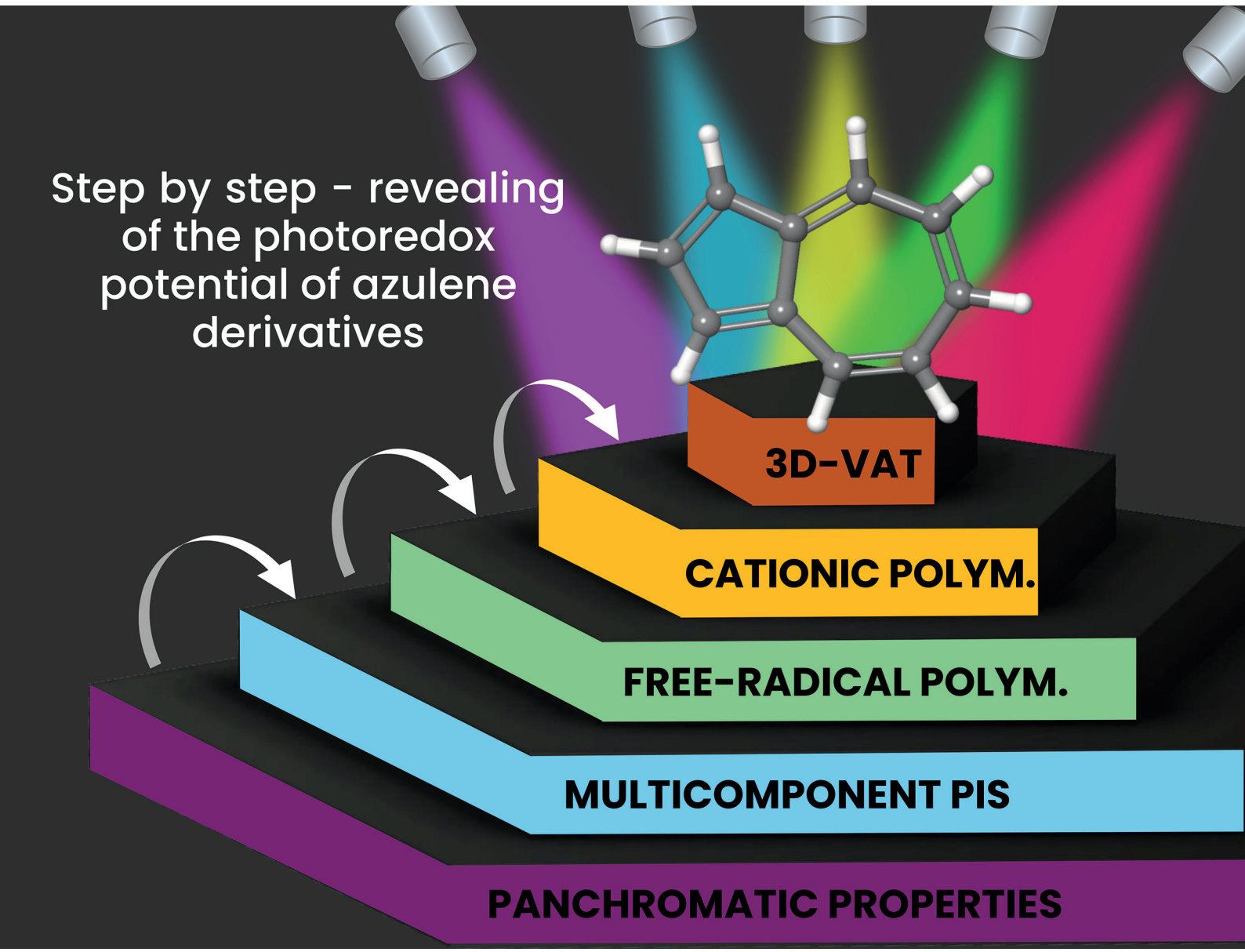

ISSN 1759-9962

ROYAL SOCIETY OF CHEMISTRY

PAPER

Joanna Ortyl *et al.*

Revealing the photoredox potential of azulene derivatives as panchromatic photoinitiators in various light-initiated polymerization processes

Polymer Chemistry

ROYAL SOCIETY OF CHEMISTRY

PAPER

View Article Online
View Journal | View Issue

Cite this: *Polym. Chem.*, 2024, **15**, 2931

Revealing the photoredox potential of azulene derivatives as panchromatic photoinitiators in various light-initiated polymerization processes†

Katarzyna Starzak,[a] Wiktoria Tomal,[a,b] Anna Chachaj-Brekiesz,[c] Mariusz Galek[d] and Joanna Ortyl *[a,d,e]

Received 8th March 2024,
Accepted 7th May 2024

DOI: 10.1039/d4py00275j

rsc.li/polymers

Herein, the application of previously unknown azulene derivatives as effective panchromatic photosensitizers in the visible light range in the initiation of light-induced cationic and free-radical polymerization processes was investigated. The presented azulene derivatives showed a high photoredox potential allowing the use of these compounds in two-component and three-component photoinitiating systems for various photopolymerization processes. In addition, within the scope of this manuscript, the effectiveness of using photoinitiating systems containing the proposed azulene derivatives in 3D printing to obtain three-dimensional polymer structures has been confirmed and for the first time proven in the literature.

1. Introduction

Light-induced polymerization processes are currently leading the way among methods of obtaining advanced polymeric materials due to the numerous advantages of the process, including the ability to conduct the reaction at room temperature and the lack of any need for solvents. In addition, photopolymerization is ecologically safe due to the minimal energy consumption and lesser use of toxic solvents and reduction of the amount of unreacted monomers and photoinitiators and with the selection of appropriate substrates, it is also non-toxic. Furthermore, depending on the mechanism of the ongoing reactions, it is possible to use a variety of substrates of synthetic and natural origin, and thus to obtain diversified products suitable depending on the intended use of the materials obtained to develop them with the desired parameters such as mechanical and biological properties in the context of their toxicity.[1–8] Photopolymerization is used in various fields of industry, such as photolithography to create printed circuit boards, the coating industry to photocure polymer adhesives, medicine to create functional hydrogel biomaterials, for the manufacturing of responsive and conductive materials, as well as nanostructured materials with improved mechanical properties.[9–14] In addition, the use of photopolymerization as a method for obtaining these functional polymeric materials provides an opportunity to control the ongoing process. Studying of the kinetics is possible *via* real-time monitoring such as Fourier Transform Infrared spectroscopy (FTIR), which enables the study of monomer conversion by tracking the disappearance of the characteristic vibrational bands of the interacting functional group and is one of the most widely used techniques for evaluating the conversion of functional groups of monomers and oligomers.[15–20]

Undoubtedly, a key role in the photopolymerization process is played by the photoinitiator, which is not only responsible for initiating the photopolymerization reaction, but is also responsible for the reaction kinetics and final properties of the resulting material. Photoinitiators are divided into Type I (single-component) and Type II (two- or multi-component) photoinitiators. The disadvantages of commercially used Type I photoinitiators, including the incompatibility of the absorption characteristics of photoinitiators with the emission characteristics of used light sources, result in the search for effective photoinitiating multi-component systems currently being the subject of researchers' work.[21–24] The use of a dye in such systems, that acts as a light absorber, shifts the absorption spectrum of the photoinitiating system towards longer wavelengths, greatly expanding the area of application of the photoinitiator. The dye molecule acts as a photosensitizer for the photoinitiator of the other component and it can act as an electron donor or acceptor depending on the mechanism of the reaction being carried out. The main step leading to the

[a]*Cracow University of Technology, Faculty of Chemical Engineering and Technology, Warszawska 24, 31-155 Cracow, Poland. E-mail: jortyl@pk.edu.pl*
[b]*Jerzy Haber Institute of Catalysis and Surface Chemistry, Polish Academy of Sciences, Niezapominajek 8, 30-239 Cracow, Poland*
[c]*Jagiellonian University, Faculty of Chemistry, Gronostajowa 2, 30-387 Cracow, Poland*
[d]*Photo HiTech Ltd, Bobrzyńskiego 14, 30-348 Cracow, Poland*
[e]*Photo4Chem Ltd, Lea 114, 30-133 Cracow, Poland*
† Electronic supplementary information (ESI) available. See DOI: https://doi.org/10.1039/d4py00275j

formation of initiating radicals in this type of photoinitiating system is the electron transfer process.[4,25,26] Significant progress has been made in the design and synthesis of functional dyes for efficient photoinduced polymerizations using soft light LEDs. Meanwhile, the quest for novel functional dyes that facilitate photopolymerization under blue to red LED light sources remains a difficult research problem. Dye molecules that are suitable for this purpose should strongly absorb in the spectral region corresponding to the emission wavelengths of Vis-LED light sources and should have relevant electrochemical properties.[27–32] Despite the fact that metal complexes (*e.g.*, ruthenium or iridium complexes) have been incorporated into photoinitiating systems for polymer synthesis under extremely mild irradiation conditions such as sunlight, fluorescent bulbs, or LED bulbs, these materials are either prohibitively expensive or difficult to synthesize. A more accessible solution is the use of organic dyes, which have a simpler synthesis pathway, are less toxic and exhibit improved stability and solubility.[33] Some dyes, such as acridine orange,[34] erythrosin B,[35] eosin B,[36] rhodamine B,[37] rose bengal[38] and methylene blue,[39] have previously been claimed to be employed as visible light photosensitizers. A wide range of synthetic dyes have been employed in photoinitiating systems such as acridones,[40] benzophenones,[41] camphorquinones,[42] carbazoles,[43,44] chalcones,[45] chromones,[46] coumarins,[47] cyclohexanones,[48] flavones,[49] ferrocenes,[50] helicenes,[51] naphthalimides,[52] perylenes,[53] phenothiazines,[54] porphyrins,[55] pyrenes,[56] squaraines,[57] and thioxanthones.[58] Coumarins, in particular, absorb substantially in the near-UV visible region, whereas perylenes and phthalocyanines typically absorb beyond 550–600 nm.[59–61] The tunability of their absorption spectra remains restricted for the majority of these families (coumarins, perylene, phthalocyanines); therefore a red-shift or a blue-shift of their absorptions may only be produced after significant synthetic input.[62–64]

Azulene is a naphthalene isomer composed of fused 5- and 7-membered ring structures that is named after its bright blue color. Azulene, unlike naphthalene, is a non-alternant hydrocarbon with nodal points at C-2 and C-6 of the HOMO and C-1 and C-3 of the LUMO. Because of the position of these nodes, there is less electrical repulsion in the singlet excited state (S_1), allowing for a narrow HOMO–LUMO gap. As a result, the $S_0 \rightarrow S_1$ transition results from the absorption in the visible area. In naphthalene, however, the coefficient magnitudes remain stable for each location in both the HOMO and LUMO, allowing for higher electron pair repulsion. In the same manner, there is no variation in the coefficient magnitudes of azulene's HOMO and LUMO+1, resulting in a wide S_0–S_2 gap (and hence a big S_1–S_2 gap). This results in a system in which the transition $S_2 \rightarrow S_0$ is the predominant mode of fluorescence, violating Kasha's rule.[65–71] Azulene and its derivatives have a one-of-a-kind mix of optical, luminescent, and stimuli-responsive characteristics. Because of its unusual electrical and optical characteristics, azulene has gained increased interest in recent years, and the synthesis of azulene-based functional materials has become an active subject of study. Electrochromic materials,[72] anion sensors,[73] charge-transfer complexes,[73,74] perovskite solar cells,[75] organic conductors,[76] nonlinear optical materials,[73] near-infrared resonance materials,[73,77] biology[78] and medicine[79] are just a few of the applications for azulene derivatives. Azulene derivatives are also used in organic field-effect transistors (OFETs) and organic light-emitting diodes (OLEDs).[77]

Within the framework of this manuscript, we have presented eight previously undiscovered azulene derivatives and proposed their use in multi-component photoinitiating systems for various types of polymerization reactions. Spectroscopic characterization studies confirmed the panchromatic properties of the developed compounds. On the basis of electrochemical studies and thermodynamic calculations, we proposed the use of the synthesized azulene derivatives in two- and three-component photoinitiating systems for cationic and free-radical polymerization reactions. The effectiveness of these photoinitiating systems was confirmed using Fourier-transform infrared spectroscopy in real-time (real-time FTIR). In addition, we have proven for the first time the feasibility of using azulene derivatives as photosensitizers to obtain three-dimensional polymeric materials using additive technologies, more specifically vat 3D printing using digital light processing (DLP) technology.

2. Materials and methods

2.1. Materials

A series of eight newly-synthesised azulene derivatives: 1-bromo-3-(4-methylsulfanylphenyl)azulene (**Az1**), 1,3-bis(4-methylsulfanylphenyl)azulene (**Az2**), 4-(3-bromoazulen-1-yl) benzonitrile (**Az3**), 4-[3-(4-cyanophenyl)azulen-1-yl]benzonitrile (**Az4**), 4-[3-[4-(trifluoromethyl)phenyl]azulen-1-yl]benzonitrile (**Az5**), 1-(4-methylsulfanylphenyl)-3-(4-nitrophenyl)azulene (**Az6**), 1-(4-nitrophenyl)-3-[4-(trifluoromethyl)phenyl]azulene (**Az7**), 1,3-bis[4-(trifluoromethyl)phenyl]azulene (**Az8**), shown in Fig. 1 were synthesised and evaluated for their role as photosensitizers in cationic and free-radical photopolymerization processes. The pathway for the synthesis of these compounds, along with full NMR and LCMS characterization, is presented in the ESI.† Commercially available azulene and guaiazulene (both from Sigma Aldrich) were also studied for their potential usability in photoinitiating systems.

Triethylene glycol divinyl ether (TEGDVE, from Sigma Aldrich) and 3,4-epoxycyclohexylmethyl 3,4-epoxy-cyclohexanecarboxylate (CADE, from Lambson) were used as a model vinyl ether monomer and epoxide monomer respectively, for cationic polymerization. Trimethylolpropane triacrylate (TMPTA, from Ambeed) was used as a model monomer for free radical photopolymerization. Proposed azulene derivatives were used in this study in two- or three-component photoinitiating systems with various components, namely: bis(4-*t*-butylphenyl)-iodonium hexafluorophosphate (IOD, from Lambson), *N*-vinylcarbazole (NVK, from Sigma Aldrich), tris(trimethylsilyl)silane (TTMSS, from Sigma Aldrich), *N*-methyl diethanola-

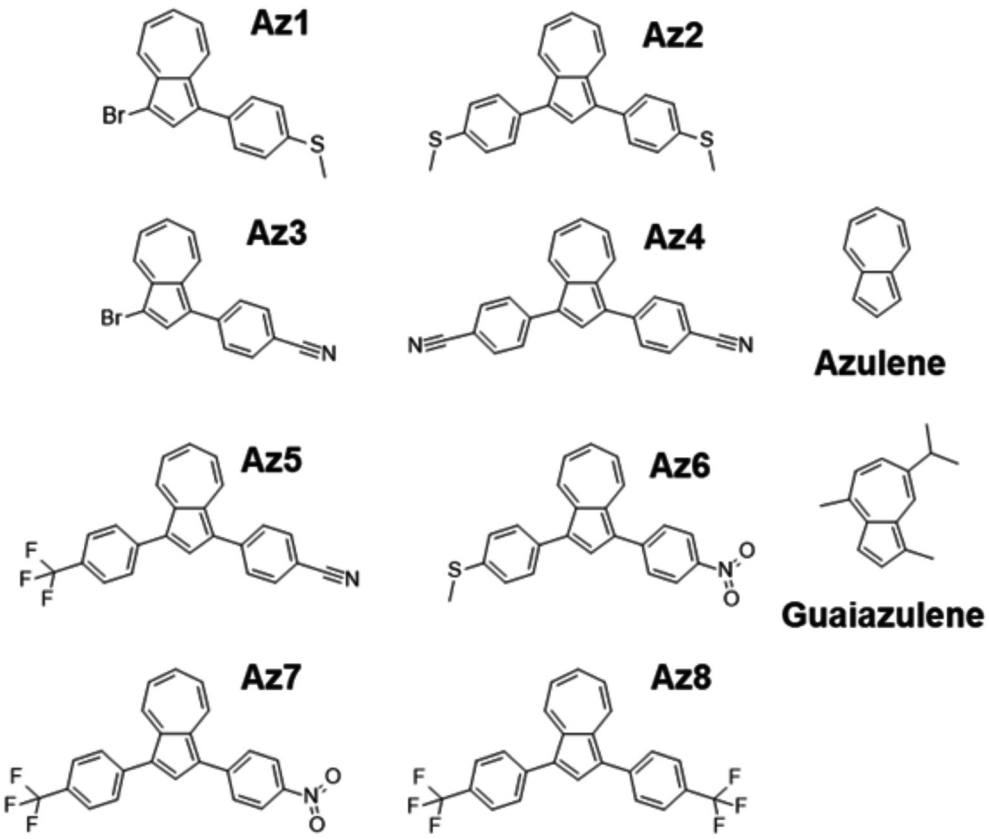

Fig. 1 Structures of azulene, guaiazulene and eight new azulene derivatives investigated in this study.

mine (MDEA from Sigma Aldrich) and 2-bromoisobutyryl bromide (BIBB, from TCI). Structures of the used chemicals are shown in the ESI in Fig. S.55–S.62.†

2.2. Absorption and fluorescence characteristics

A TEC-X2 spectrometer (from StellarNet, Inc., Tampa, FL, USA), equipped with a broadband SL5 deuterium halogen light source (from StellarNet, Inc., Tampa, FL, USA), was used for the investigation of absorbance properties of azulene derivatives in acetonitrile, at 25 °C. Measurements were carried out in a quartz cuvette with an optical path length of 10 mm.

A FluoroMax-4P spectrofluorometer (from Horiba, Kyoto, Japan) was used in order to investigate the emission and excitation spectra of all the compounds in acetonitrile. Experiments were conducted using a quartz cuvette with an optical path length of 10 mm.

2.3. Electrochemical determination of oxidation and reduction potentials

The oxidation (E_{ox} against Ag/AgCl) and reduction potentials (E_{red} *vs.* Ag/AgCl) of azulene and its derivatives were determined using cyclic voltammetry – electrochemical analyzer M161 and electrode stand M164 (from MTM-ANKO, Poland). Tetrabutylammonium hexafluorophosphate (0.1 M) (from Sigma Aldrich) was used as a supporting electrolyte, a silver chloride electrode (Ag/AgCl) was used as a reference, and a platinum disc was applied as the working electrode. The process parameters are as follows: a scan rate of 0.1 V s^{-1}, ferrocene was employed as a reference and potentials were calculated using half peak potentials. The Gibbs free energy ΔG_{et} for an electron transfer between the components of the photoinitiating system was calculated from the obtained oxidation and reduction potentials using the following formula:

$$\Delta G_{et} = F\left[E_{ox} \cdot \frac{D}{D^{\bullet+}} - E_{red} \cdot \frac{A^{\bullet-}}{A}\right] - E_{00} - \frac{Ze^2}{\varepsilon a} \qquad (1)$$

where E_{ox} ($D/D^{\bullet+}$) is the oxidation potential of the electron donor, E_{red} ($A^{\bullet-}/A$) – the reduction potential of the electron acceptor, E_{00} – the excited state energy, and ($Ze^2/\varepsilon a$) the electrostatic interaction energy for the initially formed ion pair. The parameter ($Ze^2/\varepsilon a$) is negligible in polar solvents. The excited state energy was determined from the excitation and emission spectra using a FluoroMax-4P spectrofluorometer (Horiba, Kyoto, Japan). All spectra were recorded at varied excitation wavelengths in the range of 200–800 nm.

2.4. Steady-state photolysis of azulene derivatives

A photolysis experiment was carried out for acetonitrile solutions of azulene and all of the examined derivatives. The

sample was exposed to UV–LED–365 nm (M365L2, Thorlabs Inc., USA) emitting at 365 nm wavelength and (CW = 0.7 A (54.23 mW cm^{-2})), current, for 30 min. The light source was powered using a Thorlabs Inc., USA DC2200 regulated power supply. Throughout the exposure duration, the UV-VIS spectra were acquired using a broadband beam from a UV/VIS deuterium-halogen light source (SL5, StellarNet USA).

2.5. Monitoring the photopolymerization processes by real-time FT-IR

The kinetics of light-induced polymerization processes were studied using the real-time FT-IR technique with a Thermo Scientific FT-IR^{i10} NICOLET™ spectrometer with a horizontal adapter (Waltham, MA, USA). The monomer conversion was calculated based on the changes in the absorbance of the examined sample, specifically the decrease in the absorbance of peaks responsible for functional groups or bonds engaged in the photopolymerization process, using eqn (2):

$$\text{Conversion}\,[\%] = \left(1 - \frac{A_{\text{After}}}{A_{\text{Before}}}\right) \times 100\% \qquad (2)$$

where A_{After} is the monitored band's area, and A_{Before} is the starting value of the monitored band's area.

The characteristic absorbance peaks for the investigated monomers are described below in detail for each photopolymerization individually. Due to the fact that proposed azulene derivatives exhibit panchromatic properties, the following light sources were used for photopolymerization studies: 405 nm M405LP1 Vis-LED (CW = 1.4 A (29.73 mW cm^{-2})), 415 nm M415LP1 Vis-LED (CW = 2.0 A (32.51 mW cm^{-2})), 450 nm M450LP1 Vis-LED (CW = 2.0 A (36.67 mW cm^{-2})), 475 nm M470L3 Vis-LED (CW = 1.0 A (12.88 mW cm^{-2})), 505 nm M505L3 Vis-LED (CW = 1.0 A (7.93 mW cm^{-2})), 530 nm M530L3 Vis-LED (CW = 1.0 A (6.94 mW cm^{-2})) and 565 nm M565L3 Vis-LED (CW = 1.0 A (17.44 mW cm^{-2})) from Thorlabs Inc., Tampa, FL, USA. A DC2200 controlled power supply (from Thorlabs Inc., Tampa, FL, USA) was used to regulate the power of the light. The sample was irradiated for 10 seconds after the process began. The distance between the irradiation sources and the formulations was 2.1 cm.

2.5.1. Panchromatic light-sensitization properties of azulene. A real-time FT-IR technique was employed to determine the panchromatic light-sensitization properties of azulene. The compositions consisted of the acrylate monomer TMPTA with the corresponding photoinitiating system: MDEA (3.0 wt%), bromide (2.0 wt%) and azulene (0.5 wt%). Cationic photopolymerization was also conducted using the vinyl ether monomer TEGDVE and a different three-component photoinitiating system: NVK (3.0 wt%), IOD (2.0 wt%) and azulene (0.5 wt%). Mechanisms corresponding to both photoinitiating systems are shown in Figure S.63 in the ESI.† All of the photocurable compositions were studied under the irradiation of different light sources mentioned above. The laminated samples (between two polypropylene films; thickness 25 μm) were deposited on a horizontal holder in an FT-IR spectrometer and were irradiated. For both photopolymerization processes, the progress of the reaction was monitored at 1620 cm^{-1} for 800 s, at a constant temperature of 25 °C.

2.5.2. Photoredox processes in the initiation of free-radical photopolymerization. Compositions consisting of the TMPTA monomer and MDEA (3.0 wt%), bromide (2.0 wt%) and azulene and all of its derivatives (0.5 wt%) were investigated. Quantities of the initiating system were recalculated relative to the amount of the monomer. A series of reference processes were performed for mixtures of the TMPTA monomer with MDEA (3.0 wt%) and bromide (2.0 wt%) used together and separately. The experiments were conducted using two different light sources: LED@405 nm with a current of 1.4 A (29.73 mW cm^{-2}) and LED@450 nm with a current of 2.0 A (36.67 mW cm^{-2}). The laminated samples (between two polypropylene films; thickness 25 μm) were deposited on a horizontal holder in an FT-IR spectrometer and were irradiated. The evolution of the double bond of acrylate was monitored at 1635 cm^{-1} for 800 s, at a constant temperature of 25 °C.

2.5.3. Photoredox processes in the initiation of cationic photopolymerization

Cationic ring opening photopolymerization process of epoxy monomers. The kinetics of cationic photopolymerization processes were studied using compositions based on two monomers, CADE or TEGDVE. The epoxy monomer CADE was used together with NVK (3.0 wt%), TTMSS (3.0 wt%), IOD (2.0 wt%) and azulene derivatives (0.5 wt%). Amounts of photo-initiating systems were calculated according to the quantity of the used monomer. For reference, similar compositions but without azulene derivatives were tested. The mechanisms corresponding to these photoinitiating systems are shown in Fig. 2a and b. As an irradiation source, an LED@450 nm with a current of 2.0 A (36.67 mW cm^{-2}) was applied. The experiments were carried out on a BaF_2 pallet (thickness 25 μm) and the epoxy content was continuously monitored under air at about 790 cm^{-1} for 800 s, at a constant temperature of 25 °C.

Cationic photopolymerization of the vinyl ether monomer. For compositions based on the vinyl ether monomer TEGDVE following initiation systems were used: MDEA (3.0 wt%), IOD (2.0 wt%) and azulene derivatives (0.5 wt%). Quantities of initiating systems were recalculated in relation to the amount of the used monomer. The initiation mechanism with the proposed photoinitiating systems can be found in Fig. 2d. As an irradiation source an LED@450 nm with a current of 2.0 A (36.67 mW cm^{-2}) was applied. The laminated samples (between two polypropylene films; thickness 25 μm) were deposited on a horizontal holder in an FT-IR spectrometer and were irradiated. The evolution of the double bond was monitored at 1620 cm^{-1} for 800 s, at a constant temperature of 25 °C.

2.6. 3D printing experiments

In order to obtain 3D printed objects a Lumen X+™ printer (from CellInk Inc., USA, supplied by Sygnis SA, Poland) was used. The printer uses digital light processing (DLP) technology and is equipped with a projector with a 405 nm light emission wavelength. Autodesk Fusion 360 was used to create

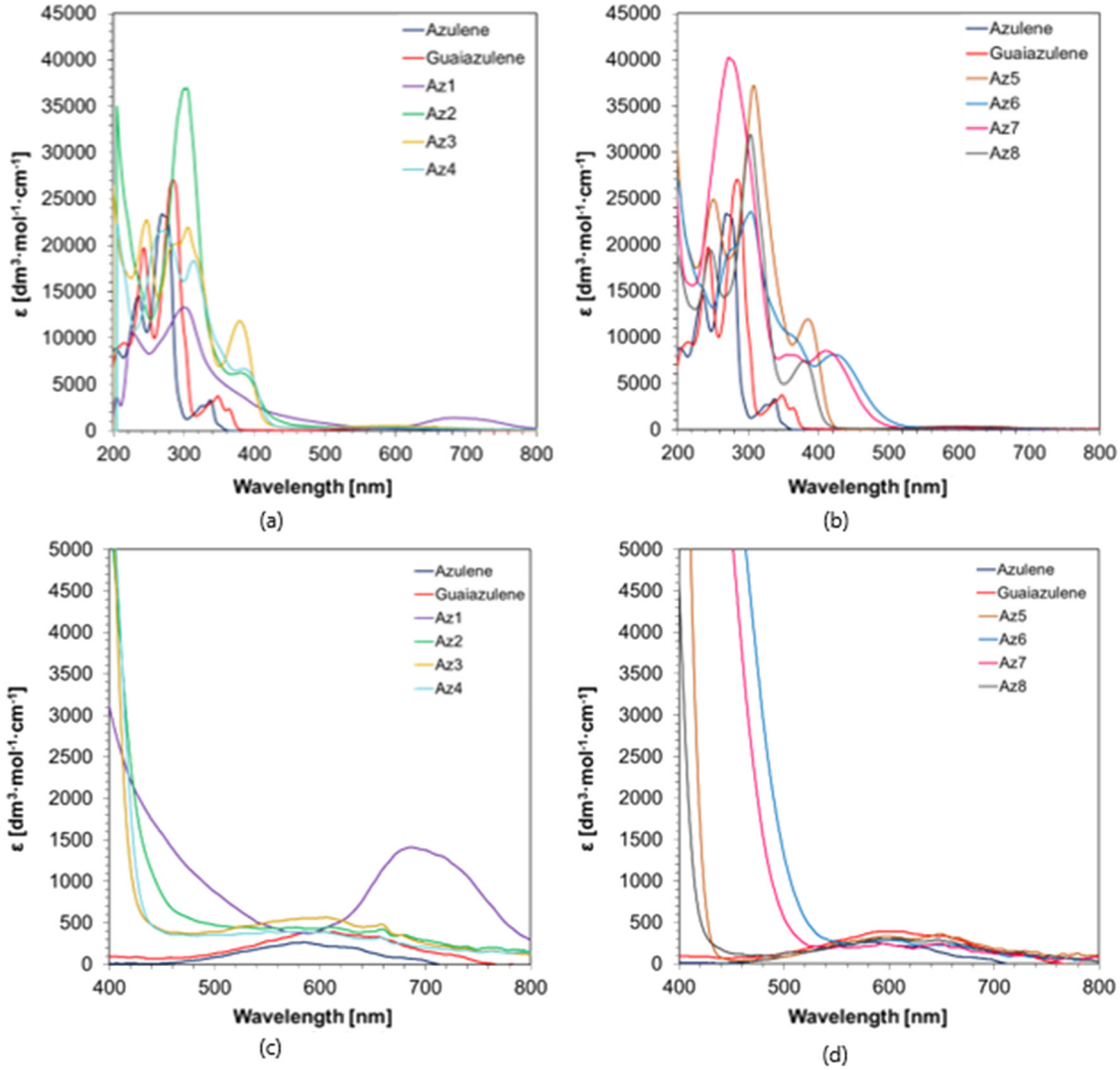

Fig. 2 UV-visible absorption spectra of azulene, guaiazulene, (a) **Az1–Az4** derivatives and (b) **Az5–Az8** derivatives in acetonitrile shown in the 200 nm–800 nm range and zoomed in the 400 nm–800 nm range for (c) **Az1–Az4** derivatives and (d) **Az5–Az8** derivatives.

the printed designs. The numerical optical microscope DSX-HRSU (OLYMPUS Corporation, Japan) equipped with a DSX10-SXLOB3X objective lens using a magnification of 42–420× was used to examine the created 3D objects. A high-resolution scanning electron microscope Apreo 2 S LoVac (Thermo Fisher Scientific) equipped with X-ray energy dispersive spectrometers – EDS detectors UltraDry (Thermo Fisher Scientific) and Octane Elect (EDAX Ametek GmbH) – was used to produce high-resolution images of the obtained printouts.

3. Results and discussion

3.1. Determination of the spectroscopic properties of the investigated azulene derivatives

The absorption properties of the investigated azulene derivatives are shown in Fig. 2 as a function of the molar extinction coefficient against the wavelength. All of the studied compounds exhibit outstanding extinction coefficients in the visible range with ε-values exceeding almost 10 000 [$dm^3\ mol^{-1}\ cm^{-1}$] in numerous cases. Furthermore, the newly synthesized azulene derivatives have an absorption spectrum that is significantly pushed towards longer wavelengths when compared to azulene, which makes it possible to effectively use these derivatives with various light sources from a safe visible range. The λ_{onset} of these photosensitizers reaches up to even 800 nm for a lesser intensity absorption band. Because of the broad absorption range of these compounds, light sources in the UV and visible ranges up to 405 nm can be used, as well as those corresponding to further absorption bands ranging from around 450 nm to even 800 nm. The spectroscopic properties of azulene derivatives determined in acetonitrile are summarized in Table 1 – the values of the molar extinction coefficients were also determined for the wavelengths corresponding to the wavelengths emitted by the light sources used later in the study.

Table 1 Spectral characteristics of azulene derivatives studied in acetonitrile

Acronym	$\varepsilon_{365\ nm}$ [dm^3 mol^{-1} cm^{-1}]	$\varepsilon_{405\ nm}$ [dm^3 mol^{-1} cm^{-1}]	$\varepsilon_{455\ nm}$ [dm^3 mol^{-1} cm^{-1}]	$\varepsilon_{470\ nm}$ [dm^3 mol^{-1} cm^{-1}]	$\varepsilon_{490\ nm}$ [dm^3 mol^{-1} cm^{-1}]	$\varepsilon_{505\ nm}$ [dm^3 mol^{-1} cm^{-1}]	$\varepsilon_{530\ nm}$ [dm^3 mol^{-1} cm^{-1}]	$\varepsilon_{565\ nm}$ [dm^3 mol^{-1} cm^{-1}]
Azulene	29	13	18	44	73	101	166	250
Guaiazulene	2315	97	83	85	108	135	208	323
Az1	4614	2600	1391	1160	926	775	556	383
Az2	6083	3933	663	570	486	469	443	445
Az3	9358	3037	388	374	392	412	471	552
Az4	6880	4102	363	355	350	361	376	397
Az5	9248	5291	47	48	90	101	184	277
Az6	10 019	7351	5450	3526	1605	849	319	255
Az7	8057	8371	3704	1953	718	355	221	199
Az8	6074	1588	125	105	127	135	206	255

3.2. Electrochemical determination of oxidation and reduction potentials

Cyclic voltammetry studies of the investigated azulene derivatives have been performed in order to determine their photo-oxidation and photo-reduction properties. Exemplary cyclic voltammetery curves for azulene derivative – **Az6** are shown in Fig. 3a and c, together with absorption and fluorescence spectra determined in acetonitrile (Fig. 3b).

New azulene derivatives have been proposed for use in photoinitiating systems, where electron transfer occurs *via* a photo-oxidation mechanism. In such a cycle, the azulene derivative acts as an electron donor and undergoes oxidation during the process. The role of the electron acceptor in this case can be played by an iodonium salt or BIBB, among others, which undergoes reduction during the process. Electrochemical experiments and thermodynamic calculations were performed to confirm the validity of the proposed systems, and the data obtained are summarized in Table 2. Compounds such as IOD[80–85] and BIBB and their analogs[3,86–89] are well known in the literature as components of initiator systems dedicated to light-induced polymerization processes.

The conventional Rehm–Weller equation was used to determine the Gibbs free energy (ΔG) based on the observed oxidation potentials of newly synthesized azulene derivatives. Because ΔG is negative, the obtained results clearly show that the photoinduced electron transfer process in the initiating system consisting of the given azulene derivatives and IOD, as well as BIBB is thermodynamically acceptable. However, the results for the Gibbs free energy obtained for IOD-based systems are slightly lower than for BIBB-based systems; therefore, it is suspected that initiating systems based on iodonium salt will be more effective.

New azulene derivatives were also proposed for initiating systems based on MDEA, NVK and TTMSS. This sort of photoinitiating system is based on electron transfer from one molecule, known as the co-initiator, to another, defined as the electron acceptor. Two-component systems including MDEA[55,94–98] or NVK[99–104] or TTMSS[91,105–108] and azulene derivatives can operate in this type of photoinitiating system along with the aforementioned compounds acting as co-initiators and being oxidized through electron transfer, and azulene derivatives acting as an electron acceptor and being reduced due to electron transfer. Electrochemical studies were performed to assess the reduction abilities of the proposed compounds in

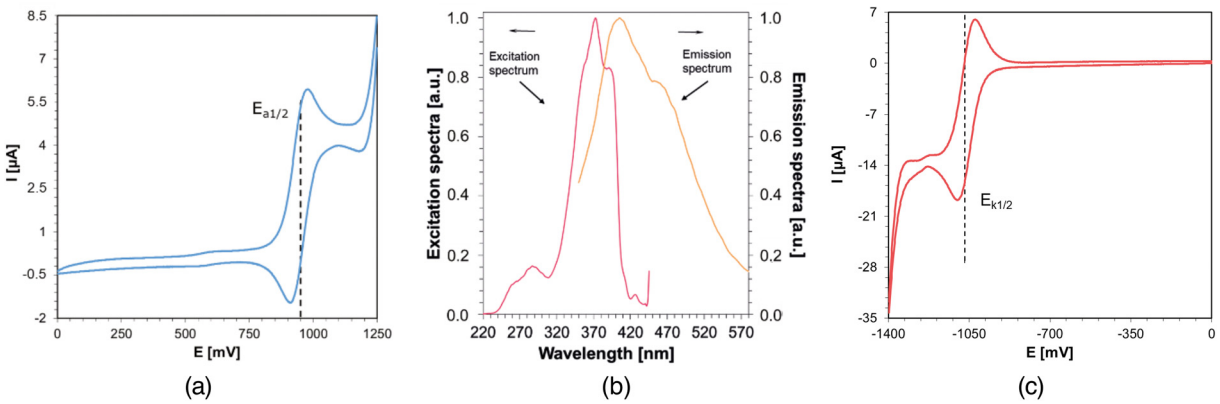

Fig. 3 (a) Cyclic voltammetry for the oxidation process (CV_{ox}, *vs.* Ag/AgCl); experiments in ACN (containing 0.1 M tetrabutylammonium hexafluorophosphate) for the **Az6** derivative; (b) absorption and fluorescence spectra for the determination of the excited singlet state energy for the **Az6** derivative; (c) cyclic voltammetry for the reduction process (CV_{red}, potential *vs.* Ag/AgCl) experiments in ACN (containing 0.1 M tetrabutylammonium hexafluorophosphate) for the **Az6** derivative.

Table 2 Electrochemical and thermodynamical properties of azulene derivatives in terms of their use in the photo-oxidation mechanism in light induces the electron transfer process calculated for compositions

	Singlet state energy	Electrochemically determined potentials		Photo-oxidation		Photo-reduction		
Acronym	E_{00} [eV]	E_{ox} [mV]	E_{red} [mV]	ΔG_{IOD} [a] [eV]	$\Delta G_{BROMDIE}$ [a] [eV]	ΔG_{MDEA} [a] [eV]	ΔG_{NVK} [a] [eV]	ΔG_{TTMSS} [a] [eV]
Azulene	3.50	987	−337	−1.87	−1.71	−2.30	−1.94	−2.73
Guaiazulene	3.36	742	−348	−1.98	−1.82	−2.15	−1.79	−2.58
Az1	3.00	776	−1351	−1.58	−1.43	−0.78	−0.43	−1.21
Az2	3.13	835	−1381	−1.65	−1.50	−0.88	−0.53	−1.31
Az3	3.06	1057	−1249	−1.36	−1.20	−0.95	−0.59	−1.37
Az4	3.05	1123	−1295	−1.29	−1.13	−0.89	−0.54	−1.32
Az5	3.22	1091	−1325	−1.49	−1.33	−1.03	−0.68	−1.46
Az6	2.95	951	−1035	−1.36	−1.20	−1.05	−0.70	−1.48
Az7	2.98	1105	−1069	−1.23	−1.08	−1.05	−0.69	−1.47
Az8	3.24	1068	−1355	−1.53	−1.37	−1.02	−0.67	−1.45

[a] Calculated from the classical Rehm–Weller equation: $\Delta G_{et} = F[E_{ox}(D/D^{\bullet+}) - E_{red}(A^{\bullet-}/A)] - E_{00} - \left(\frac{N_A e^2}{4\pi\varepsilon_0\varepsilon_r a}\right)$. E_{ox} $(D/D^{\bullet+})$ – electron donor's electrochemically determined oxidation potential (0.864 V for MDEA *vs.* Ag/AgCl);[90] (1.219 V for NVK *vs.* Ag/AgCl); (0.436 V for TTMSS *vs.* Ag/AgCl).[91] E_{red} $(A^{\bullet-}/A)$ – electron acceptor's electrochemically determined reduction potential (−0.64 V for IOD *vs.* Ag/AgCl);[92,93] (−0.798 V for BIBB *vs.* Ag/AgCl). E_{00} – sensitizer's singlet state energy determined based on emission and excitation spectra.

order to establish their utility in these types of photoinitiating systems, and the results are presented in Table 2.

Gibbs free energy (ΔG) has been determined using the measured reduction potentials for the analyzed azulene derivatives. Because ΔG is negative, the electron transfer processes in the photoinitiating systems consisting of azulene derivatives and MDEA/NVK/TTMSS respectively are thermodynamically acceptable. The most favourable, *i.e.* lowest, Gibbs free energy values were obtained for systems based on TTMSS, and the least favourable ones from the thermodynamical point of view are systems with NVK for which the highest values were obtained. Nonetheless, the acquired values allow us to conclude that the examined derivatives are suitable for all of the studied initiating systems. In addition, it is possible to claim that the studied derivatives can also find application in three-component photoinitiating systems based on both reducing and oxidizing compounds mentioned before.

3.3. Investigation of photopolymerization processes by real-time FT-IR

Considering that azulene and its derivatives have very broad absorption spectra up to 800 nm, FT-IR experiments were carried out using an LED light source in the visible range to determine the potential of the tested derivatives to initiate light-induced free radical and cationic polymerization processes.

3.3.1. Panchromatic light-sensitization properties of azulene. The aim of the study was to exploit the panchromatic spectroscopic properties of azulene to photosensitize the iodonium salts for free-radical and cationic photopolymerization processes using different light sources compatible with the absorption range of this compound. For the determination of panchromatic light-sensitization properties of azulene for free-radical polymerization processes the following acrylate composition was used: TMPTA with an initiating system containing azulene (0.5%), MDEA (3.0%) and BIBB (2.0%) and the results along with the photo-redox mechanism of the given initiating systems are shown in Fig. 4. For cationic polymerization the vinyl ether monomer TEGDVE with an initiating system containing azulene (0.5%), NVK (3.0%) and IOD (2.0%) was applied, and the obtained results along with the photo-redox mechanism of the given initiating systems are shown in Fig. 5. An overview of the used diodes containing their wavelengths along with the light intensity at the sample can be found in the ESI in Table S.3.†

Final conversion of acrylate and vinyl ether monomers, along with other data such as the photopolymerization rate determined as the slope of the kinetic curve, induction time, absorption intensity for azulene at a given wavelength, light source and light intensity on the sample, are summarized in Table 3. In the case of azulene, as the wavelength increases, the absorption value of electromagnetic radiation also increases. This relationship is partly reflected in the conversion results obtained for the compositions tested using light sources of different wavelengths. However, it should be noted that the conversion results obtained for a diode emitting light at 470 nm and 505 nm reached by far the lowest values for both compositions, but this is caused by the lower intensity of light radiating on the sample combined with relatively low absorption values. Namely, in the case of diodes emitting light of a lower wavelength, there is a significantly higher light intensity value on the sample and a lower absorption value for azulene. For higher wavelengths, on the other hand, we dealt with the opposite relationship. However, the final conversion values obtained at 405–470 nm and 530–565 nm are significant.

Taking into account the obtained results and the determined values, such as the slope of the curve and the induction time, the conclusion can be drawn that azulene shows good panchromatic light-sensitization properties, thanks to that it

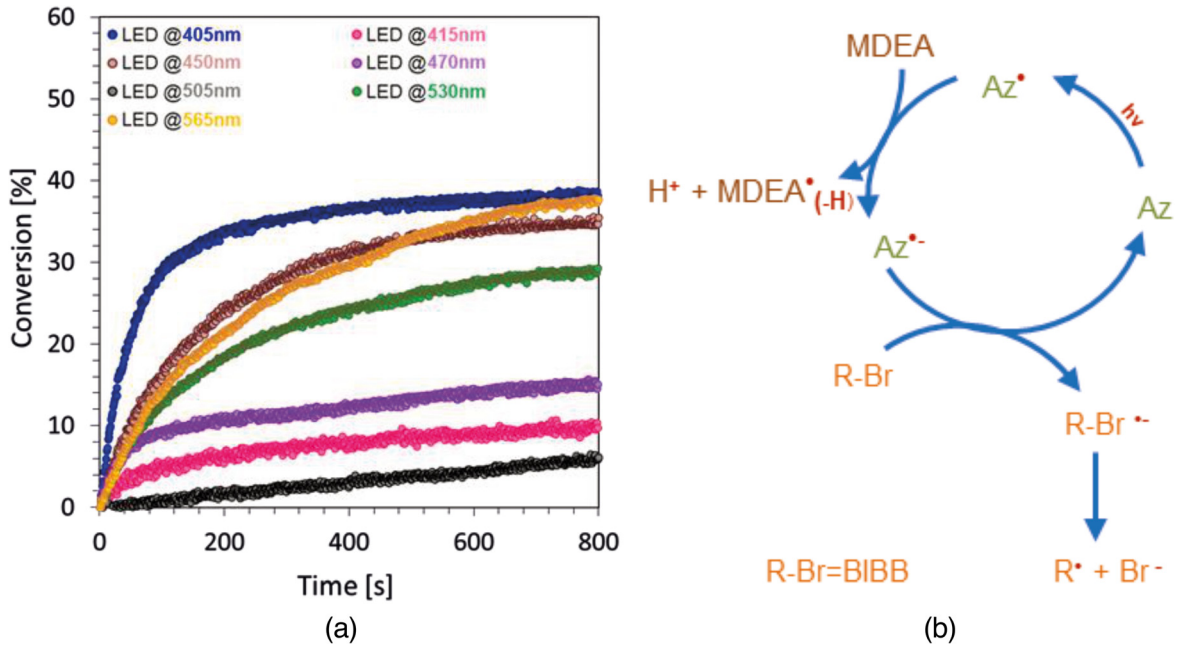

Fig. 4 (a) Free-radical photopolymerization profiles (double conversion *vs.* time) for the acrylate monomer TMPTA and the three-component initiating system: azulene (0.5%), MDEA (3.0%) and BIBB (2.0%). (b) A catalytic cycle involving azulene derivatives (Az) as photocatalysts for polymerization in an oxidative and reductive process.

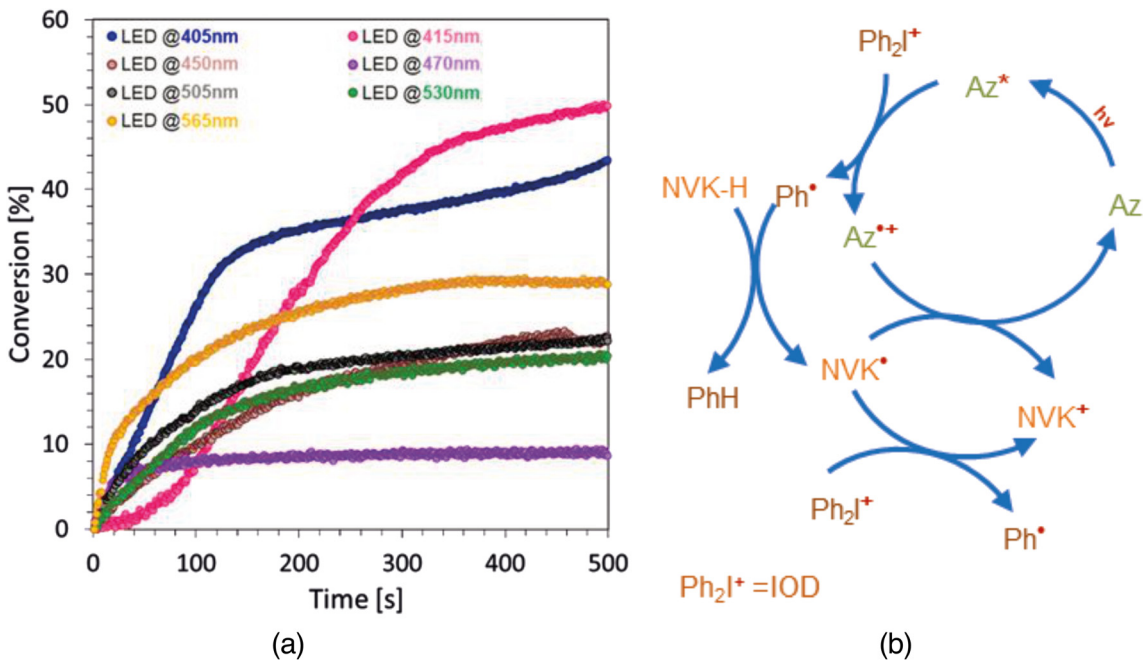

Fig. 5 (a) Cationic photopolymerization profiles (double conversion *vs.* time) for the vinyl ether monomer TEGDVE and the three-component initiating system: azulene (0.5%), NVK (3.0%) and IOD (2.0%). (b) A catalytic cycle involving azulene derivatives (Az) as photocatalysts for polymerization in an oxidative and reductive process.

can act effectively as a photosensitizer in the case of processes carried out using LEDs with wavelengths in the range of 405 nm to 565 nm, which allows the use of safer light sources for potential applications of this type of composition.

3.3.3. Determination of the suitability of photoinitiating systems containing azulene derivatives for initiating cationic photopolymerization reactions. The suitability of using azulene and its derivatives as photosensitizers for cationic

Table 3 Summary of acrylate and vinyl monomer conversion values compared with the basic parameters of the light sources used during the photopolymerization

Composition	Conversion of the monomer (α) [%]	$d\alpha/dt$ [s^{-1}]	Molar extinction coefficient corresponding to the emission wavelength of the light source [a. u.]	Source of light [nm]	Intensity [mW cm^{-2}]
Azulene (0.5%), MDEA (3%), BROMIDE (2%), TMPTA	39	0.472	13	405	29.7
	11	0.043	18	415	32.5
	36	0.189	44	450	36.7
	16	0.146	73	470	12.9
	6	0.010	101	505	7.9
	29	0.132	166	530	6.9
	38	0.150	250	565	17.4
Azulene (0.5%), NVK (3%), IOD (2%), TEGDVE	44	0.280	13	405	29.7
	50	0.219	18	415	32.5
	23	0.105	44	450	36.7
	9	0.096	73	470	12.9
	23	0.167	101	505	7.9
	21	0.126	166	530	6.9
	30	0.205	250	565	17.4

$d\alpha/dt$ – the slope of the kinetic curve of the photopolymerization process.

polymerization processes was tested using compositions based on the vinyl ether monomer TEGDVE or the epoxy monomer CADE together with the respective initiating systems. The components of these systems were as follows, for the vinyl monomer: azulene derivative (0.5%), IOD (2.0%) and MDEA (3.0%), and for the epoxy monomer: azulene derivative (0.5%), IOD (2.0%), TTMSS (3.0%) or NVK (3.0%). Results for the photopolymerization of the vinyl ether monomer can be found in Fig. 6a and for the expoxy monomer in Fig. 7a. Kinetic profiles obtained for the studied compositions are shown in Figure S.64 for the vinyl ether monomer and Figure S.65 for the epoxy monomer in the ESI.†

The highest conversion values for the tested vinyl monomer-containing formulations reaching up to 50% for **Az1** and **Az2** derivatives. In the case of the **Az2** derivative, the high conversion result as well as its ability to act as an electron donor can be explained as a combined effect of both the significant value of the molar extinction coefficient at the studied wavelength (405 nm) and the obtained lowest value of the Gibbs free energy for the photo-oxidation process among the tested derivatives, the obtained kinetic profiles are shown in Fig. 6b. However, when using a three-component photoinitiating system with the **Az2** derivative, uncontrolled polymerization in the vial occurred. The reason for this may be the combined effect of the reactivity of the **Az2** derivative and the addition of MDEA, due to which the number of active sites in the reaction medium increases. A summary of the conversion of vinyl ether monomer-based compositions is shown in Table S.4 in the ESI.†

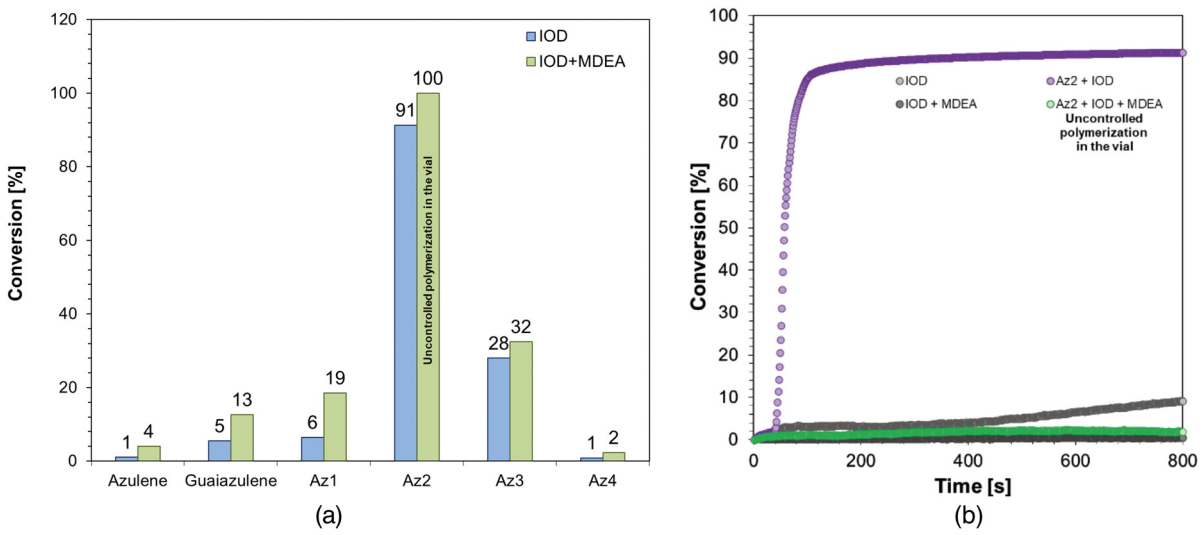

Fig. 6 (a) Comparison of maximum conversions of the vinyl ether monomer during the photopolymerization process occurring according to the cationic mechanism obtained using various initiating systems containing azulene derivatives obtained during irradiation with a light-emitting diode with a wavelength of 405 nm; (b) cationic photopolymerization profiles (double conversion *vs.* time) for the vinyl ether monomer TEGDVE and photoinitiating systems consisting of **Az2** (0.5%), MDEA (3.0%) and IOD (2.0%), accordingly.

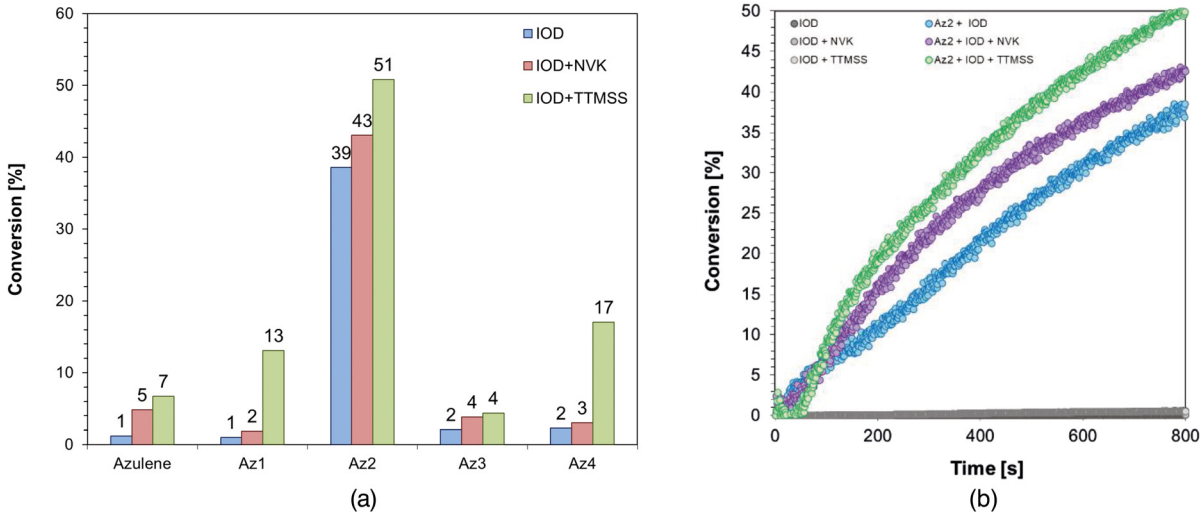

Fig. 7 (a) Comparison of maximum conversions of the epoxy monomer during the photopolymerization process occurring according to the cationic mechanism obtained using various initiating systems containing azulene derivatives obtained during irradiation with a light-emitting diode with a wavelength of 450 nm; (b) cationic photopolymerization profiles (double conversion *vs.* time) for the epoxy monomer CADE and photoinitiating systems consisting of **Az2** (0.5%), NVK (3.0%), TTMSS (3.0%) and IOD (2.0%), accordingly.

The efficiency of initiating cationic ring-opening photopolymerization (ROP) processes using the developed multicomponent photoinitiating systems based on azulene derivatives was also investigated. The results of these studies are shown in Fig. 7a.

Considering the conversion results obtained for compositions with the epoxy monomer CADE, it can be concluded that the most effective systems are the ones containing the **Az2** derivative for which the kinetic profiles are shown in Fig. 7b. This is explained by the high values of both photo-oxidation and photoreduction obtained for this derivative compared to the synthesized compounds, as well as high value of molar extinction coefficient at the tested wavelength. The **Az2** derivative in the case of such systems can act both as a reducing agent and as an oxidant agent in the photo-initiating system accompanied by appropriate compounds in the form of IOD, NVK or TTMSS. A summary of the conversions for all the epoxy monomer compositions evaluated can be found in Table S.5 in the ESI.†

3.3.2. Determination of the suitability of photoinitiating systems containing azulene derivatives for initiating free-

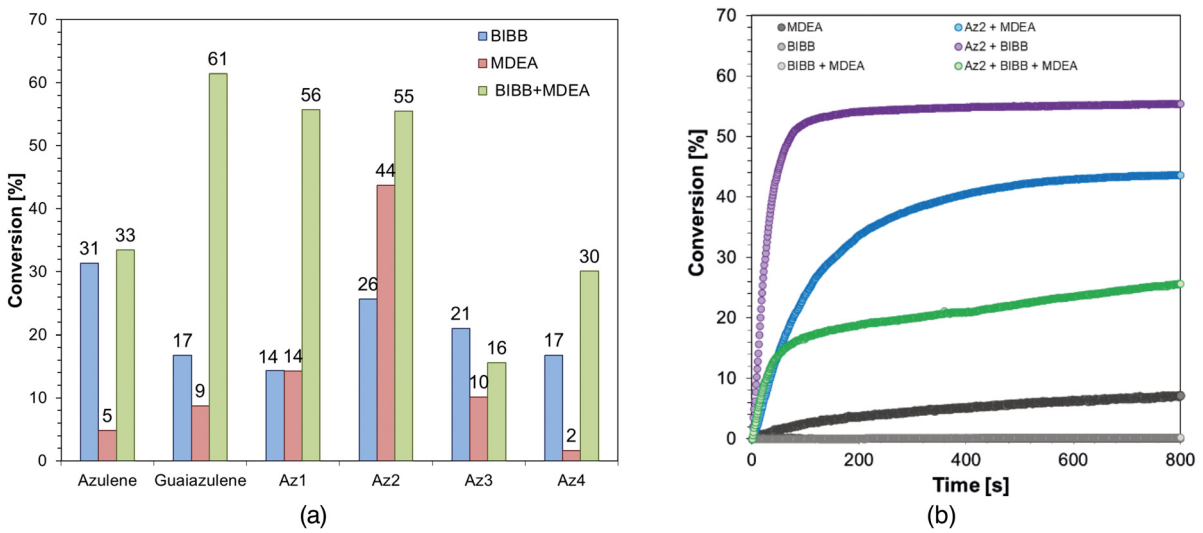

Fig. 8 (a) Comparison of maximum conversions of the acrylate monomer during the photopolymerization process occurring according to the radical mechanism obtained using various initiator systems containing azulene derivatives obtained during irradiation with a light-emitting diode with a wavelength of 405 nm; (b) free-radical photopolymerization profiles (double conversion *vs.* time) for the acrylate monomer TMPTA and photoinitiating systems consisting of **Az2** (0.5%), BIBB (2.0%), and MDEA (3.0%), accordingly.

radical photopolymerization reactions. The suitability of using azulene and its derivatives as photosensitizers for free-radical photopolymerization processes was tested using compositions based on the acrylate monomer TMPTA. The components of these systems were as follows: azulene derivative (0.5%), BIBB (2.0%) and MDEA (3.0%). The conversion results for the studied formulations obtained for free-radical polymerization using a 405 nm light source are shown in Fig. 8a and Table S.6 in the ESI† along with kinetic profiles for all the tested compositions in Figure S.66,† while the corresponding results, using a 450 nm light-emitting diode, are shown in Fig. 9a and Table S.7 in the ESI† along with kinetic profiles for all the tested compositions in Figure S.67.† Kinetic profiles obtained for compositions based on the **Az2** derivative are shown in Fig. 8b for measurements using a light source with a wavelength of 405 nm and in Fig. 9b for measurements using a light source with a wavelength of 450 nm.

In the case of studies using compositions where the process occurs according to a free-radical mechanism, it can be noted that the highest conversion rates for three-component compositions were obtained for the commercial derivative Guaiazulene and for a new derivative with the acronym **Az1**. For both of these compounds, thermodynamic calculations yielded sufficiently low Gibbs free energy values for both photoreduction and photooxidation, from which their effectiveness in photosensitizing the described light-initiated polymerization process follows. Comparable results were obtained for compositions using the **Az2** derivative, while this effect has already been described above in the case of cationic compositions. Moreover, the results obtained for the photo-

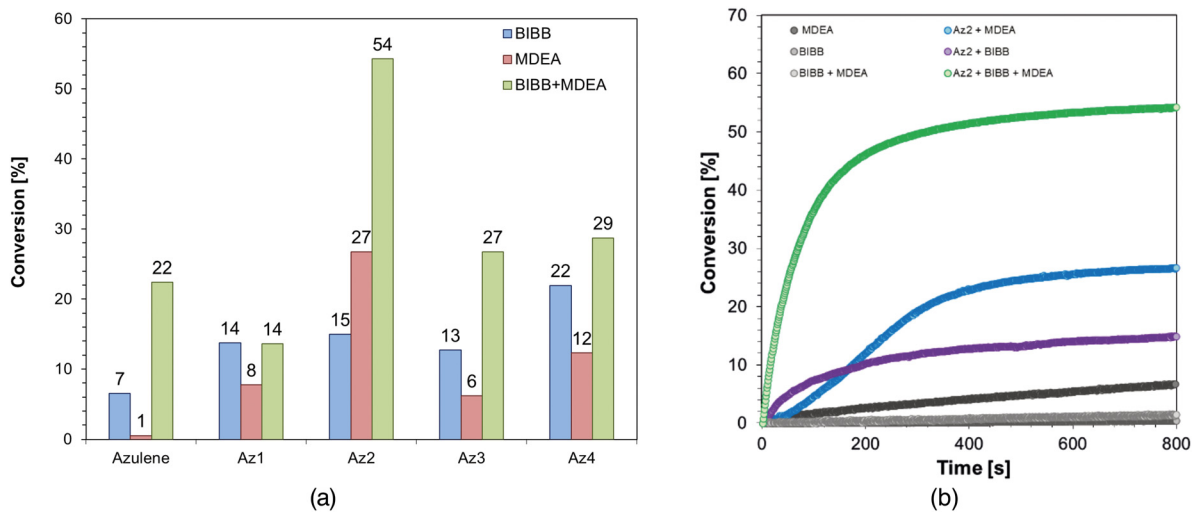

Fig. 9 (a) Comparison of maximum conversions of the acrylate monomer during the photopolymerization process occurring according to the radical mechanism obtained using various initiator systems containing azulene derivatives obtained during irradiation with a light-emitting diode with a wavelength of 450 nm; (b) free-radical photopolymerization profiles (double conversion *vs.* time) for the acrylate monomer TMPTA and photoinitiating systems consisting of **Az2** (0.5%), BIBB (2.0%), and MDEA (3.0%), accordingly.

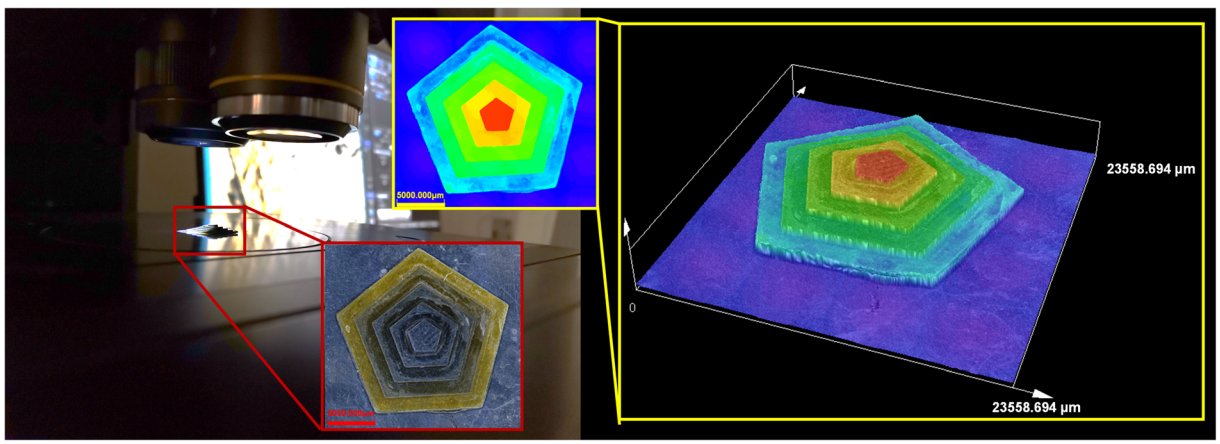

Fig. 10 Images of the first 3D object obtained by 3D printing including a panoramic photo of the print, a panoramic photo showing the differences in the heights of individual layers and 3D visualization of the heights of individual parts of the print.

polymerization process occurring according to the free-radical mechanism are higher than for the cationic process, which is influenced by the higher reactivity of the acrylate monomers.

In the case of using a longer wavelength of 450 nm to irradiate the tested compositions during real-time FT-IR measurements, the final conversion values obtained for the tested compositions based on the acrylate monomer reached lower values than those in the case of using light of a shorter wavelength which is directly related to the values of the molar extinction coefficient characterizing these sensitizers, obtained for both wavelengths. This value is the highest for the **Az1** derivative, while the conversion results come out most favourably in the case of using the derivative with the acronym **Az2** as one of the components of the initiating system, but in this case the values of the Gibbs free energy reached lower values which is more beneficial.

3.4. Determining the suitability of photoinitiating systems containing azulene derivatives in 3D-VAT printing technology

The compositions whose photopolymerization process proved to be the most efficient in the above studies, that is, the one based on the vinyl monomer TEGDVE and a two-component initiating system containing a derivative with the acronym **Az2** (0.5%) and IOD (2.0%), was selected for manufacturing 3D objects by vat 3D printing using DLP technology. A LUMEN X+™ printer with a projector that emits light of 405 nm wavelength with the power set at 80%, with an exposure time of 30 seconds for each layer and 150 seconds for the base layers, was

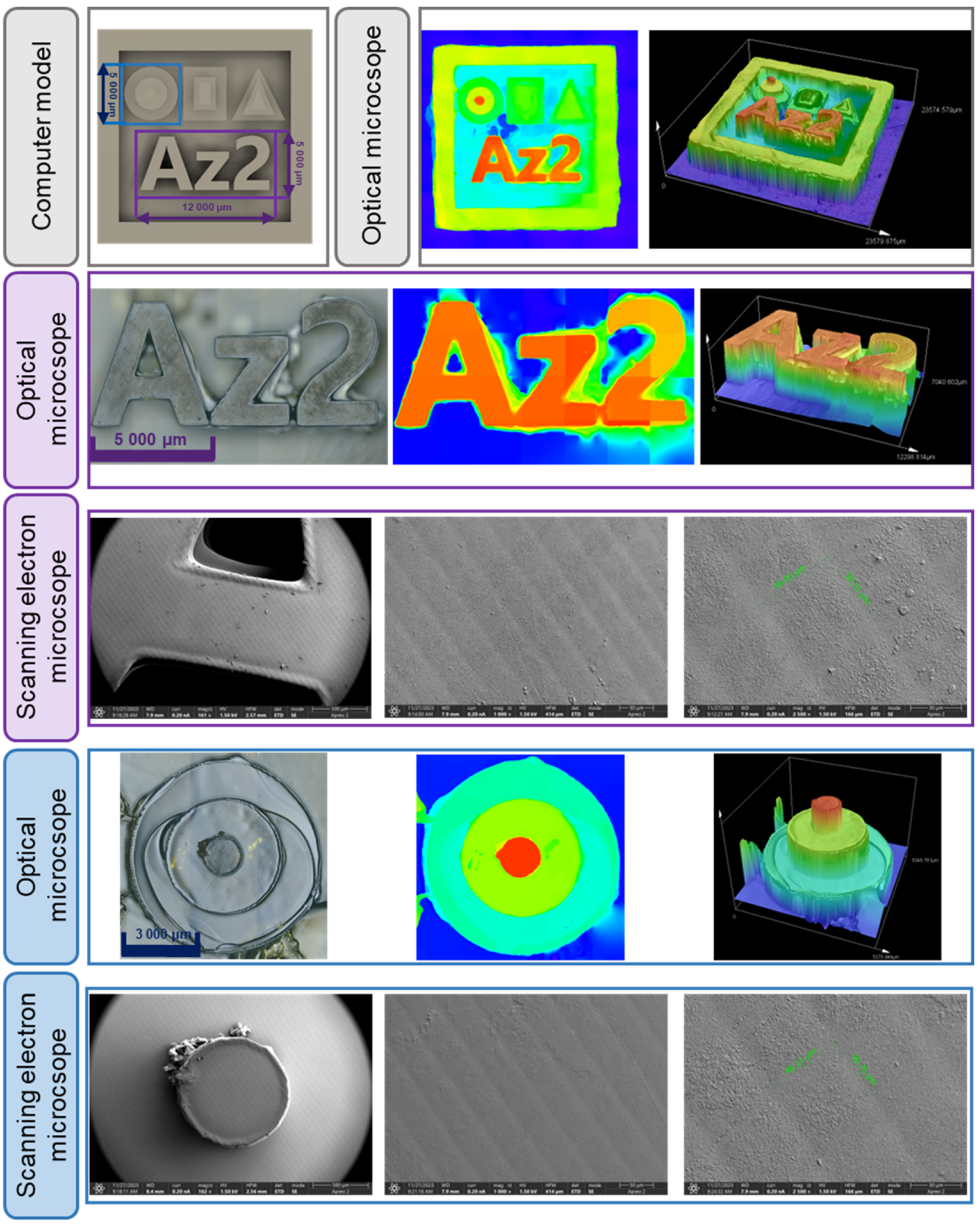

Fig. 11 Photographs of a print made from an **Az2** derivative-based resin obtained using an optical microscope and a scanning electron microscope.

used to manufacture the 3D printouts. In the first stage, an attempt was made to print a simple material with the shape of a low-height pentagon in the form of a pyramid. Fig. 10 contains optical microscope images obtained for the first printed object. The completed print has excellent resolution, which is particularly evident in the 3D visualization obtained by analysing the print with an optical microscope as well as the SEM images shown in the ESI in Figure S.68.† It can be seen that the respective heights of the individual layers are maintained as included in the initial digital design.

The print presented in Fig. 10 shows slight local over-cross-linking in the bottom layer, and some of the resins that remained on the print could not be washed off because they had time to pre-polymerize between printing and removing the print from the platform, which from our observations is due to the extended exposure time, especially for the first layer, though it had to be extended due to the poor adhesion of the print to the printer's work platform. A potential solution to this problem would seem to reduce the power of the projector or reduce the exposure time. However, conducting these steps would involve a lack of adhesion of the print to the working platform, which was tested before the final print was made. Satisfied with the results of the printing of a simple computer model using the proposed composition, we attempted to print another polymeric material, which was characterized by an increased number of precision parts, which were used to determine the final suitability of the developed azulene derivative based resin for use in 3D printing. The overall print shown in Fig. 11 was 20 mm wide, 20 mm long and 4 mm high. However, the dimensions of the individual elements were much smaller. The **Az2** inscription was 3 mm high, 12 mm wide and 5 mm long, while the pyramid, on the other hand, having the same overall height, was designed so that each step was 1 mm high where the diameters were respectively 5 mm for the largest circle, 3 mm for the middle circle and 1 mm for the smallest circle. The preservation of such intricate details at good resolution demonstrates the satisfactory performance of the developed resin based on azulene derivative **Az2**. It should also be noted that this is the first study of its kind to show the applicability of azulene and its derivatives as components of an initiating system for obtaining high-resolution 3D prints.

Using scanning electron microscopy, it was possible to actually determine the resolution of the printout. As shown in Fig. 11, the pixels are clearly visible, and their dimensions are about 50 μm × 50 μm, indicating that the selected composition based on an initiator system containing an **Az2** derivative acting as a photosensitizer of iodonium salt can be successfully used for 3D printing.

4. Conclusions

Within the framework of this article, 8 new azulene derivatives were synthesized. Comprehensive spectroscopic studies, together with electrochemical investigations, made it possible to determine the spectroscopic, electrochemical, and thermodynamic properties of the studied compounds and to prequalify them as potential components of multicomponent initiating systems. Four of the eight newly synthesized azulene derivatives (1-bromo-3-(4-methylsulfanylphenyl)azulene (**Az1**), 1,3-bis(4-methylsulfanylphenyl)azulene (**Az2**), 4-(3-bromoazulen-1-yl)benzonitrile (**Az3**), and 4-[3-(4-cyanophenyl)azulen-1-yl]benzonitrile (**Az4**)) proved to be suitable for use as photosensitizers for polymerization processes occurring according to both free-radical and cationic mechanisms. FT-IR studies conducted in the first part confirmed the panchromatic light-sensitization properties of azulene in the context of the application of diodes in the visible range, while the second part made it possible to determine the suitability of the studied derivatives for photoinitiating systems for free-radical and cationic photopolymerization processes. The most promising of all the tested derivatives turned out to be the derivative with the acronym **Az2**, whose performance is related to the structure of this compound, and mainly the presence of two sulphur atoms in its structure. This shows that the inclusion of electron-donor groups to the core allows one to improve the photosensitizing properties of azulene derivatives. These compounds are difficult to optimize however, with unusual absorption properties. Nevertheless, the electron lifetimes in the triplet state are mostly not sufficient to effectively photosensitize the described processes. These properties are improved, however, when electron-donors are added. This leads to a wide absorption range of this derivative and high values of the molar extinction coefficient for the applied diodes emitting the selected wavelength, as well as low values of the Gibbs free energy for both photo-oxidation and photo-reduction processes. Therefore, a composition with this derivative was selected to assess the applicability of this type of composition in 3D printing. As a result of the 3D printing tests, 3D objects with definitely satisfactory resolution were obtained, so it can be concluded that the newly synthesized azulene derivatives can be used as components of initiating systems in photocurable compositions for 3D printing. In addition, the excellent properties of the developed azulene sensitizers provide a good perspective for the development of 3D-VAT printing technology, which is currently focused on devices using 405 nm light, but looking at the development of this technology, the proposed derivatives will be good candidates for photoinitiating polymerization reactions in printers equipped with sources of visible light reaching beyond 405 nm.

Author contributions

K. S.: conceptualization, data curation, validation, methodology, investigation, formal analysis, writing – original draft, and writing – review and editing; W. T.: conceptualization, data curation, validation, methodology, investigation, formal analysis, writing – original draft, and writing – review and editing; A. Ch. B.: organic synthesis and validation; J. O.: conceptualization, funding acquisition, investigation, methodology, supervision, validation, writing – original draft, and writing – review and editing.

Data availability

Data will be made available on request.

Conflicts of interest

The authors declare no conflict of interest.

Acknowledgements

This research was funded by the NCN project OPUS ("Emerging strategy approaches for the design and functionalization of carbon dots as multifunctional, dynamic, green system photoinitiators and photocatalysts involved in photopolymerisation processes"), Grant No. UMO-2021/41/B/ST5/04533.

References

1 M. Chen, M. Zhong and J. A. Johnson, Light-Controlled Radical Polymerization: Mechanisms, Methods, and Applications, *Chem. Rev.*, 2016, **116**, 10167–10211, DOI: 10.1021/ACS.CHEMREV.5B00671/ASSET/IMAGES/MEDIUM/CR-2015-006712_0045.GIF.

2 A. Bagheri and J. Jin, Photopolymerization in 3D Printing, *ACS Appl. Polym. Mater.*, 2019, **1**, 593–611, DOI: 10.1021/ACSAPM.8B00165/ASSET/IMAGES/LARGE/AP-2018-00165Y_0007.JPEG.

3 M. Mueller, C. Bandl and W. Kern, Surface-Immobilized Photoinitiators for Light Induced Polymerization and Coupling Reactions, *Polymers*, 2022, **14**, 608, DOI: 10.3390/POLYM14030608.

4 W. Tomal and J. Ortyl, Influence of a non-reactive additive on the photocuring and 3D-VAT printing processes of PEGDA: Complementary studies, *Eur. Polym. J.*, 2022, **180**, 111588, DOI: 10.1016/J.EURPOLYMJ.2022.111588.

5 L. Pierau, C. Elian, J. Akimoto, Y. Ito, S. Caillol and D.-L. Versace, *Bio-sourced Monomers and Cationic Photopolymerization: The Green combination towards Eco-Friendly and Non-Toxic Materials*, 2022, https://www.sciencedirect.com/science/article/pii/S0079670022000156 (accessed April 16, 2023).

6 M. Topa, F. Petko, M. Galek, M. Jankowska, R. Popielarz and J. Ortyl, Difunctional 1H-quinolin-2-ones as spectroscopic fluorescent probes for real-time monitoring of photopolymerisation process and photosensitizers of fluorescent photopolymer resin in 3D printing, *Eur. Polym. J.*, 2021, **156**, 110612, DOI: 10.1016/J.EURPOLYMJ.2021.110612.

7 Y. Lee, C. Boyer and M. Sang Kwon, Photocontrolled RAFT polymerization: past, present, and future, *Chem. Soc. Rev.*, 2023, **52**, 3035–3097, DOI: 10.1039/D1CS00069A.

8 D. A. Corbin and G. M. Miyake, Photoinduced Organocatalyzed Atom Transfer Radical Polymerization (O-ATRP): Precision Polymer Synthesis Using Organic Photoredox Catalysis, *Chem. Rev.*, 2022, **122**, 1830–1874, DOI: 10.1021/ACS.CHEMREV.1C00603/ASSET/IMAGES/MEDIUM/CR1C00603_0045.GIF.

9 S. Park, W. Shou, L. Makatura, W. Matusik and K. (Kelvin) Fu, 3D printing of polymer composites: Materials, processes, and applications, *Matter*, 2022, **5**, 43–76, DOI: 10.1016/J.MATT.2021.10.018.

10 M. Topa-Skwarczyńska, A. Świeży, D. Krok, K. Starzak, P. Niezgoda, B. Oksiuta, W. Wałczyk and J. Ortyl, Novel Formulations Containing Fluorescent Sensors to Improve the Resolution of 3D Prints, *Int. J. Mol. Sci.*, 2022, **23**, 10470, DOI: 10.3390/IJMS231810470/S1.

11 E. Hola, M. Topa, A. Chachaj-Brekiesz, M. Pilch, P. Fiedor, M. Galek and J. Ortyl, New, highly versatile bimolecular photoinitiating systems for free-radical, cationic and thiol–ene photopolymerization processes under low light intensity UV and visible LEDs for 3D printing application, *RSC Adv.*, 2020, **10**, 7509–7522, DOI: 10.1039/C9RA10212D.

12 M. Noworyta, M. Topa-Skwarczyńska, P. Jamróz, D. Oksiuta, M. Tyszka-Czochara, K. Trembecka-Wójciga and J. Ortyl, Influence of the Type of Nanofillers on the Properties of Composites Used in Dentistry and 3D Printing, *Int. J. Mol. Sci.*, 2023, **24**, 10549, DOI: 10.3390/IJMS241310549/S1.

13 X. Xia, C. M. Spadaccini and J. R. Greer, Responsive materials architected in space and time, *Nat. Rev. Mater.*, 2022, **7**, 683–701, DOI: 10.1038/s41578-022-00450-z.

14 V. A. Bobrin, Y. Yao, X. Shi, Y. Xiu, J. Zhang, N. Corrigan and C. Boyer, Nano- to macro-scale control of 3D printed materials via polymerization induced microphase separation, *Nat. Commun.*, 2022, **13**, 1–10, DOI: 10.1038/s41467-022-31095-9.

15 D. S. Esen, F. Karasu and N. Arsu, The investigation of photoinitiated polymerization of multifunctional acrylates with TX-BT by Photo-DSC and RT-FTIR, *Prog. Org. Coat.*, 2011, **70**, 102–107, DOI: 10.1016/J.PORGCOAT.2010.10.010.

16 K. Sawicz-Kryniger, P. Niezgoda, P. Stalmach, K. Starzak, A. Wysocka, T. Świergosz and R. Popielarz, Performance of FPT, FTIR and DSC methods in cure monitoring of epoxy resins, *Eur. Polym. J.*, 2022, **162**, 110933, DOI: 10.1016/J.EURPOLYMJ.2021.110933.

17 P. Szymaszek, W. Tomal, T. Świergosz, I. Kamińska-Borek, R. Popielarz and J. Ortyl, Review of quantitative and qualitative methods for monitoring photopolymerization reactions, *Polym. Chem.*, 2023, **14**, 1690–1717, DOI: 10.1039/D2PY01538B.

18 P. Bednarczyk, I. Irska, K. Gziut and P. Ossowicz-Rupniewska, Novel Multifunctional Epoxy (Meth)Acrylate Resins and Coatings Preparation via Cationic and Free-Radical Photopolymerization, *Polymers*, 2021, **13**, 1718, DOI: 10.3390/POLYM13111718.

19 J. C. Steinbach, M. Schneider, O. Hauler, G. Lorenz, K. Rebner and A. Kandelbauer, A Process Analytical

Concept for In-Line FTIR Monitoring of Polysiloxane Formation, *Polymers*, 2020, **12**, 2473, DOI: 10.3390/POLYM12112473.

20 W. Tomal, P. Szymaszek, M. Bilut, R. Popielarz, T. Świergosz and J. Ortyl, meta -Terphenyls as versatile fluorescent molecular sensors for monitoring the progress of hybrid polymerization processes, *Polym. Chem.*, 2022, **13**, 4650–4665, DOI: 10.1039/D2PY00525E.

21 J. Ortyl, M. Topa, I. Kamińska-Borek and R. Popielarz, Mechanism of interaction of aminocoumarins with reaction medium during cationic photopolymerization of triethylene glycol divinyl ether, *Eur. Polym. J.*, 2019, **116**, 45–55, DOI: 10.1016/J.EURPOLYMJ.2019.03.060.

22 E. Hola, M. Pilch and J. Ortyl, Thioxanthone Derivatives as a New Class of Organic Photocatalysts for Photopolymerisation Processes and the 3D Printing of Photocurable Resins under Visible Light, *Catalysts*, 2020, **10**, 903, DOI: 10.3390/CATAL10080903.

23 W. Tomal, A. Chachaj-Brekiesz, R. Popielarz and J. Ortyl, Multifunctional biphenyl derivatives as photosensitisers in various types of photopolymerization processes, including IPN formation, 3D printing of photocurable multiwalled carbon nanotubes (MWCNTs) fluorescent composites, *RSC Adv.*, 2020, **10**, 32162–32182, DOI: 10.1039/D0RA04146G.

24 W. Tomal, D. Krok, A. Chachaj-Brekiesz, P. Lepcio and J. Ortyl, Harnessing light to create functional, three-dimensional polymeric materials: multitasking initiation systems as the critical key to success, *Addit. Manuf.*, 2021, **48**, 102447, DOI: 10.1016/J.ADDMA.2021.102447.

25 A. Balcerak, J. Kabatc-Borcz, Z. Czech and M. Bartkowiak, Latest Advances in Highly Efficient Dye-Based Photoinitiating Systems for Radical Polymerization, *Polymers*, 2023, **15**, 1148, DOI: 10.3390/POLYM15051148.

26 J. P. Fouassier, F. Morlet-Savary, J. Lalevée, X. Allonas and C. Ley, Dyes as Photoinitiators or Photosensitizers of Polymerization Reactions, *Materials*, 2010, **3**, 5130–5142, DOI: 10.3390/MA3125130.

27 K. Sun, P. Xiao, F. Dumur and J. Lalevée, Organic dye-based photoinitiating systems for visible-light-induced photopolymerization, *J. Polym. Sci.*, 2021, **59**, 1338–1389, DOI: 10.1002/POL.20210225.

28 T. F. Zhou, X. Y. Ma, W. X. Han, X. P. Guo, R. Q. Gu, L. J. Yu, J. Li, Y. M. Zhao and T. Wang, D-D-A dyes with phenothiazine-carbazole/triphenylamine as double donors in photopolymerization under 455 nm and 532 nm laser beams, *Polym. Chem.*, 2016, **7**, 5039–5049, DOI: 10.1039/C6PY00918B.

29 M. A. Tasdelen, J. Lalevée and Y. Yagci, Photoinduced free radical promoted cationic polymerization 40 years after its discovery, *Polym. Chem.*, 2020, **11**, 1111–1121, DOI: 10.1039/C9PY01903K.

30 X. ling Zuo, S. fan Wang, K. Zheng, C. Wu, D. hai Zhang, Z. gang Dong, T. fei Wang, F. Xu, J. bing Guo and Y. ye Yang, Fluorescent-brightener-mediated thiol-ene reactions under visible-light LED: A green and facile synthesis route to hyperbranched polymers and stimuli-sensitive nanoemulsions, *Dyes Pigm.*, 2021, **189**, 109253, DOI: 10.1016/J.DYEPIG.2021.109253.

31 E. Hola, A. Gruchała, R. Popielarz and J. Ortyl, Non-destructive visual inspection of photocurable coatings based on fluorescent response of naked-eye visible colorimetric and fluorescent sensors, *Eur. Polym. J.*, 2021, **160**, 110802, DOI: 10.1016/J.EURPOLYMJ.2021.110802.

32 T. Hu, H. Fu, J. Xiong and T. Wang, Benzylidene piperidones as photosensitizers for visible light photopolymerization, *J. Photochem. Photobiol., A*, 2021, **405**, 112968, DOI: 10.1016/J.JPHOTOCHEM.2020.112968.

33 P. Xiao, J. Zhang, F. Dumur, M. A. Tehfe, F. Morlet-Savary, B. Graff, D. Gigmes, J. P. Fouassier and J. Lalevée, Visible light sensitive photoinitiating systems: Recent progress in cationic and radical photopolymerization reactions under soft conditions, *Prog. Polym. Sci.*, 2015, **41**, 32–66, DOI: 10.1016/J.PROGPOLYMSCI.2014.09.001.

34 T. Nagabhushanam and M. Santappa, Dye-sensitized photopolymerization of vinyl monomers in the presence of ascorbic acid–sodium hydrogen orthophosphate complex, *J. Polym. Sci., Part A-1: Polym. Chem.*, 1972, **10**, 1511–1528, DOI: 10.1002/POL.1972.150100519.

35 X. Nan, Y. Huang, Q. Fan, J. Shao and Y. Yao, Efficient visible photoinitiator with high-spectrum stability in an acid medium for free-radical and free-radical-promoted cationic photopolymerization based on erythrosine B derivatives, *J. Appl. Polym. Sci.*, 2016, **133**, 43035, DOI: 10.1002/APP.43035.

36 P. Tigulla and U. Vuruputuri, Dye-sensitized photopolymerization of N,N′-methylenebisacrylamide by initiation with eosin-ascorbic acid system, *J. Chem. Sci.*, 2004, **116**, 115–118, DOI: 10.1007/BF02708204/METRICS.

37 H. B. Sun, T. Tanaka, K. Takada and S. Kawata, Two-photon photopolymerization and diagnosis of three-dimensional microstructures containing fluorescent dyes, *Appl. Phys. Lett.*, 2001, **79**, 1411–1413, DOI: 10.1063/1.1399312.

38 J. X. Jiang, Y. Li, X. Wu, J. Xiao, D. J. Adams and A. I. Cooper, Conjugated microporous polymers with rose bengal dye for highly efficient heterogeneous organophotocatalysis, *Macromolecules*, 2013, **46**, 8779–8783, DOI: 10.1021/MA402104H/SUPPL_FILE/MA402104H_SI_001.PDF.

39 T. Lyubimova, S. Caglio, C. Gelfi, P. G. Righetti and T. Rabilloud, Photopolymerization of polyacrylamide gels with methylene blue, *Electrophoresis*, 1993, **14**, 40–50, DOI: 10.1002/ELPS.1150140108.

40 N. S. Allen, Photoinitiators for UV and visible curing of coatings: Mechanisms and properties, *J. Photochem. Photobiol., A*, 1996, **100**, 101–107, DOI: 10.1016/S1010-6030(96)04426-7.

41 W. Schnabel, Photoinitiation of Ionic Polymerizations, *Macromol. Eng.*, 1995, 67–83, DOI: 10.1007/978-1-4615-1905-8_6.

42 M. Topa and J. Ortyl, Novel Effective Photoinitiators for the Production of Dental Fillings, *J. Photopolym. Sci.*

Technol., 2021, **34**, 259–262, DOI: 10.2494/PHOTOPOLYMER.34.259.

43 M. Sangermano, G. Malucelli, A. Priola, S. Lengvinaite, J. Simokaitiene and J. V. Grazulevicius, Carbazole derivatives as photosensitizers in cationic photopolymerization of clear and pigmented coatings, *Eur. Polym. J.*, 2005, **41**, 475–480, DOI: 10.1016/J.EURPOLYMJ.2004.10.030.

44 J. Ortyl, M. Galica, R. Popielarz and D. Bogdał, Application of a carbazole derivative as a spectroscopic fluorescent probe for real time monitoring of cationic photopolymerization, *Pol. J. Chem. Technol.*, 2014, **16**, 75–80, DOI: 10.2478/PJCT-2014-0013.

45 S. Chen, C. Qin, M. Jin, H. Pan and D. Wan, Novel chalcone derivatives with large conjugation structures as photosensitizers for versatile photopolymerization, *J. Polym. Sci.*, 2021, **59**, 578–593, DOI: 10.1002/POL.20210024.

46 M. A. Tehfe, F. Dumur, P. Xiao, B. Graff, F. Morlet-Savary, J. P. Fouassier, D. Gigmes and J. Lalevée, New chromone based photoinitiators for polymerization reactions under visible light, *Polym. Chem.*, 2013, **4**, 4234–4244, DOI: 10.1039/C3PY00536D.

47 S. Fan, X. Sun, X. He, Y. Pang, Y. Xin, Y. Ding and Y. Zou, Coumarin Ketoxime Ester with Electron-Donating Substituents as Photoinitiators and Photosensitizers for Photopolymerization upon UV-Vis LED Irradiation, *Polymer*, 2022, **14**, 4588, DOI: 10.3390/POLYM14214588/S1.

48 S. C. Wang, Y. H. Wu, J. Bin Hsieh, J. S. Ni and Y. C. Chen, Triphenylamine based benzylidene ketones as visible-light-absorbing Type II photoinitiators for free radical photopolymerization, *J. Photochem. Photobiol., A*, 2023, **443**, 114870, DOI: 10.1016/J.JPHOTOCHEM.2023.114870.

49 A. Al Mousawi, P. Garra, F. Dumur, B. Graff, J. P. Fouassier and J. Lalevée, Flavones as natural photoinitiators for light mediated free-radical polymerization via light emitting diodes, *J. Polym. Sci.*, 2020, **58**, 254–262, DOI: 10.1002/POL.20190044.

50 F. Dumur, Recent advances on ferrocene-based photoinitiating systems, *Eur. Polym. J.*, 2021, **147**, 110328, DOI: 10.1016/J.EURPOLYMJ.2021.110328.

51 A. Al Mousawi, F. Dumur, P. Garra, J. Toufaily, T. Hamieh, F. Goubard, T. T. Bui, B. Graff, D. Gigmes, J. Pierre Fouassier and J. Lalevée, Azahelicenes as visible light photoinitiators for cationic and radical polymerization: Preparation of photoluminescent polymers and use in high performance LED projector 3D printing resins, *J. Polym. Sci., Part A: Polym. Chem.*, 2017, **55**, 1189–1199, DOI: 10.1002/POLA.28476.

52 M. Rahal, H. Mokbel, B. Graff, V. Pertici, D. Gigmes, J. Toufaily, T. Hamieh, F. Dumur and J. Lalevée, Naphthalimide-Based Dyes as Photoinitiators under Visible Light Irradiation and their Applications: Photocomposite Synthesis, 3D printing and Polymerization in Water, *ChemPhotoChem*, 2021, **5**, 476–490, DOI: 10.1002/CPTC.202000306.

53 F. Dumur, Recent advances on perylene-based photoinitiators of polymerization, *Eur. Polym. J.*, 2021, **159**, 110734, DOI: 10.1016/J.EURPOLYMJ.2021.110734.

54 D. Xu, X. Zou, Y. Zhu, Z. Yu, M. Jin and R. Liu, Phenothiazine-based charge-transfer complexes as visible-light photoinitiating systems for acrylate and thiol-ene photopolymerization, *Prog. Org. Coat.*, 2022, **166**, 106772, DOI: 10.1016/J.PORGCOAT.2022.106772.

55 L. Breloy, V. Brezová, S. Richeter, S. Clément, J. P. Malval, S. Abbad Andaloussi and D. L. Versace, Bio-based porphyrins pyropheophorbide a and its Zn-complex as visible-light photosensitizers for free-radical photopolymerization, *Polym. Chem.*, 2022, **13**, 1658–1671, DOI: 10.1039/D1PY01714D.

56 J. V. Crivello and F. Jiang, Development of pyrene photosensitizers for cationic photopolymerizations, *Chem. Mater.*, 2002, **14**, 4858–4866, DOI: 10.1021/CM020722K/ASSET/IMAGES/LARGE/CM020722KF00009.JPEG.

57 P. Xiao, F. Dumur, T. T. Bui, F. Goubard, B. Graff, F. Morlet-Savary, J. P. Fouassier, D. Gigmes and J. Lalevée, Panchromatic photopolymerizable cationic films using indoline and squaraine dye based photoinitiating systems, *ACS Macro Lett.*, 2013, **2**, 736–740, DOI: 10.1021/MZ400316Y/SUPPL_FILE/MZ400316Y_SI_001.PDF.

58 E. Hola, P. Fiedor, A. Dzienia and J. Ortyl, Visible-Light Amine Thioxanthone Derivatives as Photoredox Catalysts for Photopolymerization Processes, *ACS Appl. Polym. Mater.*, 2021, **3**, 5547–5558, DOI: 10.1021/ACSAPM.1C00886/ASSET/IMAGES/LARGE/AP1C00886_0008.JPEG.

59 C. Pigot, G. Noirbent, D. Brunel and F. Dumur, Recent advances on push–pull organic dyes as visible light photoinitiators of polymerization, *Eur. Polym. J.*, 2020, **133**, 109797, DOI: 10.1016/J.EURPOLYMJ.2020.109797.

60 E. Hola and J. Ortyl, Pyrylium salt as a visible-light-induced photoredox catalyst for polymer and organic synthesis – Perspectives on catalyst design and performance, *Eur. Polym. J.*, 2021, **150**, 110365, DOI: 10.1016/J.EURPOLYMJ.2021.110365.

61 I. Kamińska, J. Ortyl and R. Popielarz, Applicability of quinolizino-coumarins for monitoring free radical photopolymerization by fluorescence spectroscopy, *Polym. Test.*, 2015, **42**, 99–107, DOI: 10.1016/J.POLYMERTESTING.2014.12.013.

62 J. Shao, Y. Huang and Q. Fan, Visible light initiating systems for photopolymerization: status, development and challenges, *Polym. Chem.*, 2014, **5**, 4195–4210, DOI: 10.1039/C4PY00072B.

63 I. Kamińska, J. Ortyl and R. Popielarz, Mechanism of interaction of coumarin-based fluorescent molecular probes with polymerizing medium during free radical polymerization of a monomer, *Polym. Test.*, 2016, **55**, 310–317, DOI: 10.1016/J.POLYMERTESTING.2016.09.013.

64 J. Ortyl and R. Popielarz, The performance of 7-hydroxycoumarin-3-carbonitrile and 7-hydroxycoumarin-3-carboxylic acid as fluorescent probes for monitoring of cationic photopolymerization processes by FPT, *J. Appl.*

Polym. Sci., 2013, **128**, 1974–1978, DOI: 10.1002/APP.38378.

65 R. S. H. Liu and A. E. Asato, Tuning the color and excited state properties of the azulenic chromophore: NIR absorbing pigments and materials, *J. Photochem. Photobiol., C*, 2003, **4**, 179–194, DOI: 10.1016/J.JPHOTOCHEMREV.2003.09.001.

66 L. C. Murfin and S. E. Lewis, Azulene—A Bright Core for Sensing and Imaging, *Molecules*, 2021, **26**, 353, DOI: 10.3390/MOLECULES26020353.

67 V. S. Shetti, Chemical syntheses and salient features of azulene-containing homo- and copolymers, *Beilstein J. Org. Chem.*, 2021, **17**, 2164, DOI: 10.3762/BJOC.17.139.

68 A. G. Lvov and A. Bredihhin, Azulene as an ingredient for visible-light- and stimuli-responsive photoswitches, *Org. Biomol. Chem.*, 2021, **19**, 4460–4468, DOI: 10.1039/D1OB00422K.

69 H. Xin, B. Hou and X. Gao, Azulene-Based π-Functional Materials: Design, Synthesis, and Applications, *Acc. Chem. Res.*, 2021, **54**, 1737–1753, DOI: 10.1021/ACS.ACCOUNTS.0C00893/ASSET/IMAGES/LARGE/AR0C00893_0010.JPEG.

70 P. Cowper, A. Pockett, G. Kociok-Köhn, P. J. Cameron and S. E. Lewis, Azulene – Thiophene – Cyanoacrylic acid dyes with donor-π-acceptor structures. Synthesis, characterisation and evaluation in dye-sensitized solar cells, *Tetrahedron*, 2018, **74**, 2775–2786, DOI: 10.1016/J.TET.2018.04.043.

71 R. S. H. Liu, Colorful Azulene and Its Equally Colorful Derivatives, *J. Chem. Educ.*, 2002, **79**, 183, DOI: 10.1021/ED079P183.

72 H. Xin, J. Li, R. Q. Lu, X. Gao and T. M. Swager, Azulene-Pyridine-Fused Heteroaromatics, *J. Am. Chem. Soc.*, 2020, **142**, 13598–13605, DOI: 10.1021/JACS.0C06299/SUPPL_FILE/JA0C06299_SI_002.PDF.

73 C. C. Yang, L. Li, W. Q. Tian, W. Q. Li and L. Yang, Strong second order nonlinear optical properties of azulene-based porphyrin derivatives, *Phys. Chem. Chem. Phys.*, 2022, **24**, 13275–13285, DOI: 10.1039/D2CP00735E.

74 T. Shoji, A. Yamazaki, R. Katoh, K. Shimamura, R. Sakai, M. Yasunami, T. Okujima and S. Ito, Synthesis, Reactivity, and Properties of Benz[a]azulenes via the [8 + 2] Cycloaddition of 2 H-Cyclohepta[b]furan-2-ones with an Enamine, *J. Org. Chem.*, 2022, **87**, 5827–5845, DOI: 10.1021/ACS.JOC.2C00133/SUPPL_FILE/JO2C00133_SI_001.PDF.

75 N. Tzoganakis, B. Feng, M. Loizos, M. Krassas, D. Tsikritzis, X. Zhuang and E. Kymakis, Ultrathin PTAA interlayer in conjunction with azulene derivatives for the fabrication of inverted perovskite solar cells, *J. Mater. Chem. C*, 2021, **9**, 14709–14719, DOI: 10.1039/D1TC02726C.

76 T. Shoji, S. Ito and M. Yasunami, Synthesis of Azulene Derivatives from 2H-Cyclohepta[b]furan-2-ones as Starting Materials: Their Reactivity and Properties, *Int. J. Mol. Sci.*, 2021, **22**, 10686, DOI: 10.3390/IJMS221910686.

77 T. Shoji and S. Ito, The Preparation and Properties of Heteroarylazulenes and Hetero-Fused Azulenes, *Adv. Heterocycl. Chem.*, 2018, **126**, 1–54, DOI: 10.1016/BS.AIHCH.2018.02.002.

78 S. Meher and N. K. Sharma, Azulene tethered N -aryl nucleobases: synthesis, morphology and biochemical evaluations, *New J. Chem.*, 2023, **47**, 5593–5597, DOI: 10.1039/D2NJ06272K.

79 P. Bakun, B. Czarczynska-Goslinska, T. Goslinski and S. Lijewski, In vitro and in vivo biological activities of azulene derivatives with potential applications in medicine, *Med. Chem. Res.*, 2021, **30**, 834–846, DOI: 10.1007/S00044-021-02701-0/FIGURES/15.

80 F. Petko, E. Hola, M. Jankowska, A. Gruchała-Hałat and J. Ortyl, 3D-VAT printing of nanocomposites by photopolymerisation processes using amino-meta-terphenyls as visible light-absorbing photoinitiators, *Virtual Phys. Prototyp.*, 2023, **18**(1), e2244936, DOI: 10.1080/17452759.2023.2244936.

81 D. Nowak, J. Ortyl, I. Kamińska-Borek, K. Kukuła, M. Topa and R. Popielarz, Photopolymerization of hybrid monomers, Part II: Determination of relative quantum efficiency of selected photoinitiators in cationic and free-radical polymerization of hybrid monomers, *Polym. Test.*, 2018, **67**, 144–150, DOI: 10.1016/J.POLYMERTESTING.2018.02.025.

82 M. Jankowska, A. Chachaj-Brekiesz, K. Trembecka-Wójciga, A. Jarzębska, M. Topa-Skwarczyńska, M. Pilch and J. Ortyl, Novel multi-material photo-curable resins containing high-performance photoinitiating systems and nano additives dedicated to 3D-VAT printing, *Polym. Chem.*, 2023, **14**, 2088–2106, DOI: 10.1039/D2PY01583H.

83 M. Abdallah, H. Le, A. Hijazi, M. Schmitt, B. Graff, F. Dumur, T. T. Bui, F. Goubard, J. P. Fouassier and J. Lalevée, Acridone derivatives as high performance visible light photoinitiators for cationic and radical photosensitive resins for 3D printing technology and for low migration photopolymer property, *Polymer*, 2018, **159**, 47–58, DOI: 10.1016/J.POLYMER.2018.11.021.

84 S. Villotte, D. Gigmes, F. Dumur and J. Lalevée, Design of Iodonium Salts for UV or Near-UV LEDs for Photoacid Generator and Polymerization Purposes, *Molecules*, 2020, **25**, 149, DOI: 10.3390/MOLECULES25010149.

85 K. Sun, C. Pigot, H. Chen, M. Nechab, D. Gigmes, F. Morlet-Savary, B. Graff, S. Liu, P. Xiao, F. Dumur and J. Lalevée, Free Radical Photopolymerization and 3D Printing Using Newly Developed Dyes: Indane-1,3-Dione and 1H-Cyclopentanaphthalene-1,3-Dione Derivatives as Photoinitiators in Three-Component Systems, *Catalysts*, 2020, **10**, 463, DOI: 10.3390/CATAL10040463.

86 M. Ciftci, M. A. Tasdelen, W. Li, K. Matyjaszewski and Y. Yagci, Photoinitiated ATRP in inverse microemulsion, *Macromolecules*, 2013, **46**, 9537–9543, DOI: 10.1021/MA402058A/ASSET/IMAGES/LARGE/MA-2013-02058A_0005.JPEG.

87 A. Bansal, A. Kumar, P. Kumar, S. Bojja, A. K. Chatterjee, S. S. Ray and S. L. Jain, Visible light-induced surface

initiated atom transfer radical polymerization of methyl methacrylate on titania/reduced graphene oxide nanocomposite, *RSC Adv.*, 2015, **5**, 21189–21196, DOI: 10.1039/C4RA15615C.

88 P. Liu, Modification of polymeric materials via surface-initiated controlled/"living" radical polymerization, *e-Polym.*, 2007, 7(1), 062, DOI: 10.1515/EPOLY.2007.7.1.725.

89 W. M. Wan and C. Y. Pan, Atom transfer radical dispersion polymerization in an ethanol/water mixture, *Macromolecules*, 2007, **40**, 8897–8905, DOI: 10.1021/MA0712854/ASSET/IMAGES/LARGE/MA0712854F00011.JPEG.

90 E. Andrzejewska, D. Zych-Tomkowiak, M. Andrzejewski, G. L. Hug and B. Marciniak, Heteroaromatic thiols as co-initiators for type II photoinitiating systems based on camphorquinone and isopropylthioxanthone, *Macromolecules*, 2006, **39**, 3777–3785, DOI: 10.1021/ma060240k.

91 A. Balcerak, D. Kwiatkowska, K. Iwińska and J. Kabatc, Highly efficient UV-Vis light activated three-component photoinitiators composed of tris(trimethylsilyl)silane for polymerization of acrylates, *Polym. Chem.*, 2020, **11**, 5500–5511, DOI: 10.1039/D0PY00763C.

92 P. P. Romańczyk and S. S. Kurek, The Reduction Potential of Diphenyliodonium Polymerisation Photoinitiator Is Not −0.2 V vs. SCE. A Computational Study, *Electrochim. Acta*, 2017, **255**, 482–485, DOI: 10.1016/j.electacta.2017.09.166.

93 B. Strehmel, Application of NIR-photopolymers in the graphic industry: From physical chemistry to lithographic applications, *Z. Phys. Chem.*, 2014, **228**, 129–153.

94 K. Jain, J. Klier and A. B. Scranton, Photopolymerization of butyl acrylate-in-water microemulsions: Polymer molecular weight and end-groups, *Polymer*, 2005, **46**, 11273–11278, DOI: 10.1016/J.POLYMER.2005.09.065.

95 J. Wei, H. Wang, X. Jiang and J. Yin, Novel photosensitive thio-containing polyurethane as macrophotoinitiator comprising side-chain benzophenone and co-initiator amine for photopolymerization, *Macromolecules*, 2007, **40**, 2344–2351, DOI: 10.1021/MA0615304/ASSET/IMAGES/LARGE/MA0615304F00006.JPEG.

96 J. Lalevée, M. A. Tehfe, F. Dumur, D. Gigmes, N. Blanchard, F. Morlet-Savary and J. P. Fouassier, Iridium photocatalysts in free radical photopolymerization under visible lights, *ACS Macro Lett.*, 2012, **1**, 286–290, DOI: 10.1021/MZ2001753/SUPPL_FILE/MZ2001753_SI_001.PDF.

97 J. Qiu and J. Wei, Thioxanthone photoinitiator containing polymerizable N-aromatic maleimide for photopolymerization, *J. Polym. Res.*, 2014, **21**, 1–7, DOI: 10.1007/S10965-014-0559-4/SCHEMES/3.

98 M. A. Tehfe, A. Zein-Fakih, J. Lalevée, F. Dumur, D. Gigmes, B. Graff, F. Morlet-Savary, T. Hamieh and J. P. Fouassier, New pyridinium salts as versatile compounds for dye sensitized photopolymerization, *Eur. Polym. J.*, 2013, **49**, 567–574, DOI: 10.1016/J.EURPOLYMJ.2012.10.010.

99 J. Lalevée, F. Dumur, C. R. Mayer, D. Gigmes, G. Nasr, M. A. Tehfe, S. Telitel, F. Morlet-Savary, B. Graff and J. P. Fouassier, Photopolymerization of n -vinylcarbazole using visible-light harvesting iridium complexes as photoinitiators, *Macromolecules*, 2012, **45**, 4134–4141, DOI: 10.1021/MA3005229/SUPPL_FILE/MA3005229_SI_001.PDF.

100 J. Zhang, S. Wang, J. Lalevée, F. Morlet-Savary, E. S. H. Lam, B. Graff, J. Liu, F. Xing and P. Xiao, 1,2-Diketones as photoinitiators of both cationic and free-radical photopolymerization under UV (392 nm) or Blue (455 nm) LEDs, *J. Polym. Sci.*, 2020, **58**, 792–802, DOI: 10.1002/POL.20190157.

101 P. Xiao, J. Lalevée, J. Zhao, M. H. Stenzel, P. Xiao, J. Zhao, M. H. Stenzel and J. Lalevée, N-Vinylcarbazole as Versatile Photoinaddimer of Photopolymerization under Household UV LED Bulb (392 nm), *Macromol. Rapid Commun.*, 2015, **36**, 1675–1680, DOI: 10.1002/MARC.201500214.

102 A. S. Subramanian and X. 'Matthew' Hu, Heterogeneous photosensitizers: Super-efficient dual functional polydopamine nanohybrid for epoxy photopolymerization, *Polymer*, 2022, **243**, 124558, DOI: 10.1016/J.POLYMER.2022.124558.

103 J. Zhang, J. Lalevée, F. Morlet-Savary, B. Graff and P. Xiao, Photopolymerization under various monochromatic UV/visible LEDs and IR lamp: Diamino-anthraquinone derivatives as versatile multicolor photoinitiators, *Eur. Polym. J.*, 2019, **112**, 591–600, DOI: 10.1016/J.EURPOLYMJ.2018.10.021.

104 P. Xiao, F. Dumur, M. Frigoli, M. A. Tehfe, B. Graff, J. P. Fouassier, D. Gigmes and J. Lalevée, Naphthalimide based methacrylated photoinitiators in radical and cationic photopolymerization under visible light, *Polym. Chem.*, 2013, **4**, 5440–5448, DOI: 10.1039/C3PY00766A.

105 M. A. Tehfe, J. Lalevée, X. Alionas and J. P. Fouassier, Long wavelength cationic photopolymerization in aerated media: A remarkable titanocene/tris(trimethylsilyl)silane/onium salt photoinitiating system, *Macromolecules*, 2009, **42**, 8669–8674, DOI: 10.1021/MA9016696/SUPPL_FILE/MA9016696_SI_001.PDF.

106 S. M. Hell, C. F. Meyer, G. Laudadio, A. Misale, M. C. Willis, T. Noël, A. A. Trabanco and V. Gouverneur, Silyl Radical-Mediated Activation of Sulfamoyl Chlorides Enables Direct Access to Aliphatic Sulfonamides from Alkenes, *J. Am. Chem. Soc.*, 2020, **142**, 720–725, DOI: 10.1021/JACS.9B13071/SUPPL_FILE/JA9B13071_SI_001.PDF.

107 J. Lalevée, M. Peter, F. Dumur, D. Gigmes, N. Blanchard, M. A. Tehfe, F. Morlet-Savary and J. P. Fouassier, Subtle Ligand Effects in Oxidative Photocatalysis with Iridium Complexes: Application to Photopolymerization, *Chem. – Eur. J.*, 2011, **17**, 15027–15031, DOI: 10.1002/CHEM.201101445.

108 L. Song, Q. Ye, X. Ge, A. Misra and P. Spencer, Tris(trimethylsilyl)silane as a co-initiator for dental adhesive: Photo-polymerization kinetics and dynamic mechanical property, *Dent. Mater.*, 2016, **32**, 102–113, DOI: 10.1016/J.DENTAL.2015.10.013.